Angiogenic CD8 T cells from PWH induce Granzymes-dependent PAR1 activation promoting endothelial inflammation

Tong Li[1], Chinmayee Mehta[1], Cooper James[1], Jinya Chen[1], Hui Chen[1], Gerard P Ahern[2], Ziang Zhu[1], Maitane Faus Cid[1], Maryam Abdussamad[1], Shiwen Yu[1], Jai Kumar[3], Princy Kumar[3], Colleen Hadigan[4], Kyle DiVito[5], Dorian B McGavern[6], Leonid Pobezinsky[7], and Marta Catalfamo[1]

[1]Department of Microbiology and Immunology, Georgetown University School of Medicine. Washington DC, USA

[2]Department of Pharmacology and Physiology, Georgetown University School of Medicine. Washington DC, USA

[3]Division of Infectious Diseases and Travel Medicine, Georgetown University School of Medicine. Washington DC, USA

[4]Laboratory of Immunoregulation, National Institute of Allergy and Infectious Diseases, National Institutes of Health, Bethesda, MD 20892, USA

[5]Department of Biochemistry, Molecular and Cellular Biology, Georgetown University School of Medicine. Washington DC, USA

[6]Viral Immunology and Intravital Imaging Section, National Institute of Neurological Disorders and Stroke, National Institutes of Health, Bethesda, Maryland, USA

[7]Department of Veterinary and Animal Science, University of Massachusetts, Amherst, MA, USA

Abstract

In people with HIV (PWH), T cell immune activation and endothelial inflammation are contributors of the increased cardiovascular risk, however the mechanisms remain poorly understood. PAR1 connects the coagulation cascade, endothelial cells and CD8 T cells at the site of endothelial inflammation and we hypothesized that HIV driven CD8 T cell immune activation alters endothelial repair mechanisms. Endothelial repair is partially mediated by angiogenic T (T_{ang}) cells that facilitate proliferation of endothelial cells, and differentiation of endothelial progenitor cells at site of vascular injury. During LCMV infection, we identified a subset of $CD31^{high}$CD8 T cells that exhibited a long-lived memory precursor phenotype ($CD127^{+}KLRG1^{-}$) and secreted the proangiogenic cytokine vascular endothelial growth factor (VEGF) after viral control. Furthermore, in PWH, the frequencies of CD8 T_{ang} cells were reduced and showed an activated phenotype and expression of granzymes. $GZMA^{+}GZMB^{+}$CD8 T_{ang} cells correlated with atherosclerotic cardiovascular disease (ASCVD) risk. *In vitro*, granzyme dependent PAR1 activation led to calcium mobilization and secretion of proinflammatory cytokines IL-6, IL-8 and angiopoietin-2 by primary human endothelial cells. Altogether, these findings suggest that CD8 T cells are involved in immunity against viruses and endothelial homeostasis and HIV driven immune activation alters these functions.

41 **Introduction**

42 Immune activation remains the hallmark of HIV infection, despite successful suppression of
43 viremia by antiretroviral therapy (ART). HIV-associated inflammation and immune activation
44 drives cardiovascular risk, independent of traditional risk factors, duration of antiretroviral
45 treatment and CD4 counts (1-8). Compared to the general population, People with HIV (PWH)
46 have twice the risk of cardiovascular disease (9-11). The molecular pathways by which HIV drives
47 cardiovascular risk are largely unknown and multifactorial including chronic immune activation,
48 HIV persistence and translation of viral proteins, coinfections, and others (12-21). In PWH, CD8
49 T cell immune activation is associated with carotid intima-media thickness and coronary plaque
50 suggesting an interplay between CD8 T cell activation and endothelial inflammation and
51 dysfunction (6, 16-18, 22).

52 During systemic infections such as HIV, endothelial activation and injury can be mediated
53 by viral proteins as well as the host response (23, 24). We hypothesized that HIV driven CD8
54 T cell immune activation promotes endothelial inflammation altering repair mechanisms.
55 Endothelial repair, is mediated in part by angiogenic T cells (T_{ang}) that support proliferation and
56 differentiation of endothelial progenitor cells/endothelial colony forming cells (EPC/ECFC) at the
57 site of endothelial injury (25-27). T_{ang} cells were originally described in the center of endothelial
58 progenitor cell colonies isolated from human peripheral mononuclear cells (PBMCs)(25). In *in*
59 *vivo* experiments in mice $CD31^+$ T_{ang} cells support new vessel formation (25). In inflammatory
60 diseases and aging, reduced frequencies of T_{ang} cells and loss of function have been associated
61 with increased cardiovascular disease risk (25, 28, 29). However, their role in the setting of viral
62 infections remains largely unknown.

63

64 The Protease Activated Receptor 1 (PAR1) mediates the crosstalk between the coagulation
65 system, endothelium and the adaptive immune system (CD8 T cells) at sites of vascular
66 inflammation (30-33). PAR1 is one of the four members of the seven transmembrane domain G
67 protein-coupled receptor family (PAR1, PAR2, PAR3 and PAR4) (34). PAR's activation is
68 mediated by proteolytic cleavage of the N-terminus that uncovers a tethered ligand (35, 36). In
69 humans, PAR1, PAR3 and PAR4 are activated by thrombin, whereas in mice PAR3 and PAR4 are
70 the main receptor for thrombin. In addition, PAR2 is activated by trypsin, tryptase and other
71 coagulation factors (35, 37-40). Thrombin-dependent activation of PAR1 occurs by proteolytic
72 cleavage of the extracellular domain (35, 41, 42). In addition, other proteases including granzymes
73 (A, B and K) activate PAR1 although the cleavage site is not well defined (42-49). Extracellular
74 granzymes A, B and K have been shown to induce inflammation by activating PAR1 in multiple
75 cell types including neurons, fibroblast and endothelial cells (43, 45-47, 49, 50).
76 While GZMs are viewed mainly involved in cytotoxic function, non-cytotoxic and extracellular
77 activities have been reported including regulation of vascular integrity, angiogenesis, extracellular
78 matrix remodeling (51-53). In contrast to thrombin, granzymes cleavage site and the downstream
79 signaling pathways differ from thrombin leading to a non-canonical activation of PAR1 called
80 biased signal (42-49, 54, 55).
81 In this study, we evaluated whether T_{ang} cells are involved in endothelial repair following acute
82 lymphocytic choriomeningitis virus (LCMV) infection. We found that $CD31^{high}$ expressing CD8
83 T_{ang} cells increased after viral control, have a memory precursor phenotype ($KLRG1^{-}CD127^{+}$) and
84 secrete vascular endothelial growth factor (VEGF) suggesting their contribution to endothelial
85 repair. Moreover, we found that in the setting of chronic HIV infection, immune activation drives
86 a proinflammatory phenotype of CD8 T_{ang} that express granzymes. The frequencies of

87 GZMA^{+}GZMB^{+}CD8 T_{ang} are associated with the atherosclerotic cardiovascular disease (ASCVD)
88 risk. In addition, plasma levels of GZMA correlated with endothelial inflammatory markers
89 including sVCAM1 and IL-6. *In vitro* GZMs activate PAR1 favoring the secretion of
90 proinflammatory cytokines. This evidence supports the notion that HIV driven immune activation
91 alters CD8 T_{ang} cell function and chronic stimulation of this pathway may contribute endothelial
92 inflammation and the increased risk of cardiovascular disease.

93 **Material and Methods**

94 *Study Participants*

95 Participants were studied under a MedStar Georgetown University Hospital and NIAID
96 Institutional Review Board approved HIV clinical research studies. Characteristics of the study groups
97 of PWoH (n= 17) and PWH (n= 25) are described in Table 1. All study participants signed a written
98 informed consent for the collection of samples. Animal studies were conducted under Georgetown
99 University IACUC approved protocol.

100

101 *C57BL/6 f2r$^{fl/fl}$ Mice*

102 The mouse carrying a conditional floxed (fl) PAR1 (C57BL/6 F2r$^{fl/fl}$) was constructed with
103 Ingenious Targeting Laboratories (NY, USA). Exon 2 of F2r gene was conditionally targeted and it is
104 fused in frame with p2A-Tomato reporter cassette. F2r and tdTomato genes are inactivated upon Cre
105 mediated deletion between the LoxP elements. A FRT/LoxP selection ivNeo marker as homology
106 arms were included in the final targeting vector.

107 Targeted iTL IN2 (C57BL/6) embryonic stem cells were microinjected into Balb/c blastocysts.
108 Resulting chimeras with a high percentage black coat color were mated to C57BL/6 FLP mice to
109 generate Somatic Neo Deleted mice. Confirmed somatic neomycin cassette deleted mice were bred
110 with wild-type C57BL/6N mice to generate germline neomycin cassette deleted floxed PAR1 mice
111 C57BL/6 f2r$^{fl/fl}$.

112 All mice were bred and maintained under specific pathogen-free conditions at Georgetown
113 University Division of Comparative Medicine facility. All experimental procedures were conducted
114 in accordance with the guidelines and an approved protocol by Institution Animal Care and Use
115 Committee at Georgetown University. Mice between 8 to 12 weeks old were used for experiments.

116 *RT-qPCR analysis*

117 qPCR was performed to determined mRNA expression of PARs in resting murine cells. RNA was
118 obtained from magnetic isolated B, CD4 and CD8 T cells (Miltenyi Biotech, MD). RNA was extracted
119 and purified using RNeasy Mini kit (Qiagen, MD). RNA was reverse transcribed into cDNA using
120 QuantiNova Reverse Transcription kit (Qiagen, Germany). qPCR performed with QuantiNova SYBR
121 Green PCR kit in CFX Opus Real-Time PCR system (Bio-Rad, CA). Primers used: murine *F2r*
122 (NM_010169.3): forward, 5′-ATGAAAGCGTCCTGCTGGAG-3′; reverse, 5′-
123 GGACGTTCAGAGGAAGGCTG-3′; murine *F2rl1* (NM_007974.4): forward, 5′-
124 GCTGGGAGGTATCACCCTTCT-3′; reverse, 5′-CGCAGAGAACTCATCGATGGA-3′; murine
125 *F2rl2* (NM_010170.4): forward, 5′-TGCCAGTCACTGTTTGCCAA-3′; reverse, 5′-
126 CTCGGGACACTCCGCTTTTAT-3′; murine *F2rl3* (NM_007975.3): forward, 5′-
127 GACCCCCAGCATCTACGATG-3′; reverse, 5′-CAGCAGCAGTGCTTGAGAGCT-3′.
128 Housekeeping gene HPRT was used: murine HPRT (NM_013556): forward, 5′ -
129 GCGATGATGAACCAGGTTATGA- 3′; reverse, 5′ - ACAATGTGATGGCCTCCCAT - 3′
130 LCMV Glycoprotein: forward, 5′- CATTCACCTGGACTTTGTCAGACTC -3′; reverse, 5′-
131 GCAACTGCTGTGTTCCCGAAA -3′ (56, 57).

132 Ct of each sample obtained from the amplification curve was normalized to HPRT
133 and calculated ΔCt (Ct gene of interest – Ct HPRT). Results were expressed as $2^{-\Delta Ct}$ value.

134

135 *LCMV infection*

136 C57BL/6-F2r$^{fl/fl}$ mice were intravenously infected with $2x10^5$ pfu LCMV Armstrong strain. At
137 days 6 and 21 post infection (p.i.), mice were anesthetized and perfused with cold HBSS before organs
138 (lung and spleen) were collected. *In vivo* CD8 T cell depletion was performed in LCMV infected mice

139 at day 15 p.i. Mice were injected intraperitoneally with 300 μg of anti-mouse CD8α mAbs (YTS
140 169.4, BioCell, MA) or IgG2b isotype control (LTF-2, BioCell, MA). CD8 T cell depletion was
141 confirmed by flow cytometry in lung and spleen.

142 Cell suspensions from the spleens were obtained by smashing the spleens with a syringe plunger
143 in PBS and red blood cells were lysed with ACK (Gibco, MA) for 3 min on ice. After cell lysis cell
144 suspensions were passed through a 70 μm mesh, then cell counts and viability were assessed.

145 Cell suspension from the lungs were obtained by enzymatic digestion. Lungs were cut into small
146 pieces and digested using Lung Dissociation kit (Miltenyi Biotech, MD). Cell suspensions were passed
147 through a 70 μm mesh, then cell counts and viability were assessed. Total cell suspensions were used
148 to analyze endothelial cells in the lung. For T cell analysis immune cell enrichment was performed
149 using a 35% Percoll gradient. Total lung cell suspensions were centrifuged and pellets were
150 resuspended in 12 ml of 35% Percoll (Sigma, MA) and centrifuged for 15 min without a brake at 1800
151 rpm (757g) at 7 °C. Immune cell suspensions were passed through a 70 μm mesh, then cell counts and
152 viability were assessed.

153

154 *Flow cytometry:*

155 *Phenotype lymph organs and endothelial cell phenotype*: $2x10^6$ cells from spleen, lymph nodes
156 and lung cells (pre-Percoll) were stained with LIVE/DEAD (Invitrogen, CA) for 30 minutes at 4ºC.
157 Cells were incubated with a cocktail of mAbs (Table S1, panel-1 and panel-2) for 20 minutes at 4ºC.
158 Cell were washed with staining buffer (HBSS with 0.01% of NaN_3 and 0.01% of BSA) twice and
159 acquired with a BD Symphony (BD Biosciences, CA). Cells were analyzed with FlowJo (BD
160 Biosciences, CA).

161 *Cytokine secretion assay*: $2x10^6$ splenic and immune lung cells (post-Percoll) were stimulated *in*
162 *vitro* with 1 μg/mL of LCMVGp33-41 peptide (KAVYNFATC, Anaspec, CA) in the presence of 5
163 μg/mL of Brefeldin A (Sigma, MA) and 50 U/mL of rhIL-2 (National Cancer Institution, MD) for 4
164 hours at 37°C and 5% CO_2. After stimulation, cells were stained with LIVE/DEAD (Invitrogen, CA)
165 for 30 minutes at 4ºC. Cells were washed twice and incubated with surface mAbs cocktail (Table S1,
166 panel-3) for 20 min at 4ºC. Cells were fixed and permeabilized with BD Cytofix/Cytoperm solution
167 (BD Bioscience, CA) and then incubated with the mAbs cocktail for intracellular markers for 20 min
168 at 4ºC (Table S2 panel-2). Samples were acquired in a BD Symphony and analyzed with FlowJo (BD
169 Biosciences, CA).

170 *MHC class I pentamer staining*: $1x10^6$ splenic and lung immune cells from infected mice were
171 stained with H-$2D^b$ restricted LCMVGP33-41aa pentamer (H-$2D^b$-KAVYNFATC, Proimmune, UK)
172 at room temperature (22 ºC) for 10 min followed by incubation with surface mAbs cocktail (Table S1)
173 for 20 min at 4ºC. Cell suspensions were acquired in a BD Symphony (BD Biosciences, CA) and
174 analyzed using FlowJo.

175 *CD8 T_{ang} sorting and cytokine secretion*: T cells were isolated from the lungs as described above.
176 Lung cell suspensions from naïve and infected mice at day 21 p.i. were stained with a cocktail of mAbs
177 for 20 minutes at 4ºC (Table S1), and live cells were selected using Sytox Blue staining before sorting
178 (Biolegend, CA). $CD31^{high}$ and $CD31^{neg}$ CD8 T cells were sorted on a FACSAria (BD Bioscience,
179 CA). T cells were stimulated at a concentration of 300,000 cells/mL in plates with cross-linked anti-
180 CD3 and anti-CD28 mAbs (BD Bioscience, CA). After 3 days of culture, supernatants were collected
181 and cytokines (M-CSF, PDGF-A, GM-CSF, IL-2, IL-4, IL-5, IL-13, IL-17A, IL-6, IL-22, IL-9 and
182 IL-10) were measured using LEGENDplex (Biolegend, CA) following manufacturer's instructions.
183 Briefly, 25 μL of sample in duplicates were incubated with capture mAbs coated beads for 2 hours

184 followed by incubation with detection mAbs for 1 hour at room temperature in a shaker. Each sample
185 was incubated with streptavidin-PE for 30 min and acquired with a BD Symphony (BD Biosciences,
186 CA). Results were analyzed using cloud-based software Qognit (Qognit Inc, CA).

187 *Flow cytometry human peripheral blood mononuclear cells*

188 Whole blood from people without HIV PWoH (n= 17) and PWH (n= 25) were collected in BD
189 Vacutainer blood collection tube containing EDTA (BD Bioscience, CA). Whole blood was diluted
190 with PBS with 2% FBS (1:1) and loaded on the top of Ficoll-Paque (Cytiva, MA) followed by a
191 centrifugation at 400xg for 30 min at room temperature (25°C). Peripheral blood mononuclear cells
192 (PBMCs) were collected and stained with LIVE/DEAD (Invitrogen, CA) for 30 minutes at 4ºC. Cells
193 were incubated with 1μg/mL human IgG (Sigma, MO) for 10 minutes at 4ºC to block Fc receptors
194 followed by incubation with a monoclonal antibodies (mAbs) cocktail (Table S2, panel-1) for 30
195 minutes at 4ºC. Samples were acquired with a BD Symphony (BD Biosciences, CA) and analyzed
196 using FlowJo software.

197 *Measurements of cytokines and biomarkers of endothelial inflammation in plasma*

198 Plasma was obtained from whole blood collected in BD Vacutainer blood collection tubes
199 containing EDTA (BD Bioscience, CA) from PWH (n= 25) and stored at -80°C until use. Cytokines,
200 biomarkers of endothelial inflammation and granzymes (VCAM-1, IL-6, TNFα, IFNγ, sFasL, IL-2,
201 granzyme A and granzyme B) were measured using LEGENDplex (Biolegend, CA) following
202 manufacturer's instructions as described above.

203 *Unsupervised clustering analysis*

204 Multidimensional analysis was performed using Phenograph algorithm (FlowJo, CA). 10,000 of
205 manually gated lung endothelial cells ($CD326^{-}CD45^{-}CD31^{+}$) were concatenated from naïve mice and
206 infected mice at days 6 and 21 p.i. Samples acquired on different days were normalized using Mutual

207 Nearest Neighbors (MNN) (FlowJo, CA) (58). Unsupervised clusters were analyzed with Phenograph
208 (k= 100) based on surface markers (CD31, PDL1, tdTomato, CD34, CD309, VCAM-1, CD105,
209 CD90.2 and CD201). Mean fluorescence intensity of each marker for all the clusters was presented in
210 heatmap and median frequency of each cluster from naïve and infected mice were expressed as bubble
211 plots.
212
213 *Co-culture of primary human umbilical vein endothelial cells (HUVEC) and CD8 T_{ang} cells*
214 Frozen PBMCs from PWoH (n= 10) and PWH (n= 10) were thawed and rested for 2 hours. Cells
215 were incubated with 1μg/mL human IgG (Sigma, MO) for 10 minutes at 4ºC to block Fc receptors
216 followed by a cocktail of mAbs incubation for 30 minutes at 4ºC (Table S2, panel-2). Live cells were
217 selected using Sytox Blue staining before sorting (Biolegend, CA). CD8 T_{ang} cells were sorted on a
218 FACSAria (BD, CA) and centrifuged at 1000 rpm for 30 minutes. Sorted CD8 T_{ang} cells were activated
219 with anti-CD3 and anti-CD28 mAbs coated beads (Miltenyi Biotech, MD) for 3 days and expanded in
220 the presence of 50 U/mL of recombinant human (rh) IL-2 (National Cancer Institution, MD) for 14
221 days. 5,000 HUVEC and 100,000 of CD8 T_{ang} cells were resuspended in endothelial cell growth basal
222 media (Lonza, CA) and seeded in the 96 well plate in the presence or absence of anti-CD3/anti-CD28
223 mAbs coated beads (Miltenyi Biotech, MD) and incubated at 37ºC and 5% CO_2 overnight. As a
224 control, HUVEC alone was stimulated with 20 ng/mL of rhIFNγ (PeproTech, NJ) and 0.5 ng/mL of
225 rhTNFα (R&D System, MN) overnight. Cytokines in supernatant were measured using LEGENDplex
226 (Biolegend, CA) as described above.
227
228 *Tube formation assay*

229 Frozen PBMCs from PWH (n= 3) and PWoH (n= 2) were thawed and rested for 2 hours and sorted
230 as described above. Cells were incubated with 1μg/mL human IgG (Sigma, MO) for 10 minutes at
231 4ºC to block Fc receptors followed by a cocktail of mAbs incubation for 30 minutes at 4ºC (Table S2,
232 panel 2). Live cells were selected using Sytox Blue staining before sorting (Biolegend, CA). CD8 T_{ang}
233 memory cells ($CD45RA^{-}CD27^{+}$) were sorted as described above. For HIV-Gag-specific CD8 T cells,
234 PBMCs from PWH were stimulated with HIV_{gag} peptide pool (2 μg/mL, NIH AIDS Reagent Program)
235 overnight and $CD137^{+}$CD8 T cells were sorted. Sorted cells were washed twice with cold PBS and
236 labeled with 1.5 μM of CSFE (Invitrogen, CA) for 8 min at 37ºC followed by quenching with cold
237 FBS for 5 min on ice. CFSE labeled sorted cells were rested overnight. 10 μL of basement membrane
238 extract (Cultrex reduced growth factor, R&D System, MN) was applied in the inner well of 15 well
239 μ-slide chambered coverslip (ibidi, WI) and incubated for 20 min at 37°C for gelation. HUVEC and
240 CFSE labeled CD8 T_{ang} cells were resuspend in endothelial cell growth basal media (Lonza, CA) at
241 2:1 endothelial cell to T cell ratio and seeded on the top of gel in each well. Chambered coverslips
242 (Ibidi, WI) were incubated in a stage-top cell incubator at 37°C and 5% CO_2 and evaluated using Leica
243 SP8 live cell imaging (Leica, IL) at 4, 6, 8, 10 and 12 hours at 10X magnification. Analysis was
244 analyzed using the image analysis platform Wimasis (Wimasis GmbH, Germany).
245
246 *Calcium mobilization assay*
247 60,000 HUVEC were cultured on a coverslip in endothelial cell growth media (Lonza, CA) for 8
248 hours and starved with endothelial cell growth basal media-2 (EBM-2) containing 1% PBS overnight.
249 Cells were loaded for 40 min with 1 μM Fluo-4-AM (Invitrogen, Thermo Fisher Scientific) in a buffer
250 solution containing 140 mM NaCl, 4 mM KCl, 1 mM $MgCl_2$, 1.2 mM $CaCl_2$, 10 mM HEPES, and 5
251 mM glucose (pH 7.3). Cells were imaged with 20X objective using a Nikon TE2000 microscope with

252 an excitation filter of 480 ± 15 nm and an emission filter of 535 ± 25 nm. The images were captured
253 by a Retiga 3000 digital camera (QImaging) and analysis was performed offline using ImageJ.
254
255 *Granzyme- dependent PAR1 activation*
256 100,000 HUVEC were seeded a 12 well plate in endothelial cell growth media supplemented with
257 EGM-2 bullet kit overnight. Next day cells were starved in EBM-2 containing 1% FBS for 6 hours.
258 HUVEC were incubated pre-incubated with 10 μg/mL of ATAP-2 (Invitrogen, CA) or 300 nM of
259 PAR1 antagonist SCH530348 diluted in EBM-2 containing 1% FBS for 20 min at room temperature
260 (25°C). After the preincubation period, supernatants were removed from the wells, and HUVEC were
261 stimulated with 100 nM of recombinant human granzyme A (rhGZMA, Kamiya Biomedical, WA)
262 and recombinant human granzyme K (rhGZMK, Kamiya Biomedical, Japan) with fresh inhibitors at
263 the same concentration. As the positive control, HUVEC were incubated with 100 μM of PAR1
264 agonist TFLLR-NH2 (Tocris Bioscience, UK) and control peptide RLLFT-NH2 (Tocris Bioscience,
265 UK). After overnight incubation at 37°C and 5% CO_2 supernatants were collected, and cytokines were
266 measured using LEGENDplex (Biolegend, CA) as described above.
267
268 *Statistical analysis*
269 Comparisons were performed using non-parametric Mann-Whitney test or Wilcoxon test and
270 p value $\leqslant$ 0.05 was considered significant. Correlations were performed using nonparametric
271 Spearman correlation and p value $\leqslant$ 0.01 was considered significant.
272

273 **Results**

274 **PAR1 expression is modulated in virus-specific CD8 T lymphocytes during acute LCMV**
275 **infection**

276 At the site of vascular injury mediated by trauma or infection, the crosstalk between the
277 coagulation cascade, platelets, endothelial cells and CD8 T cells is mediated by thrombin
278 dependent activation of PAR1 (30-32, 35). Particularly, PAR1 signaling is involved in CD8 T cell
279 trafficking and function (30, 33). However, whether PAR1 is modulated in CD8 T cells during
280 the immune response remains to be defined.

281 We generated a PAR1 reporter mouse that allows us to evaluate PAR1 expression in CD8 T
282 cells during the course of a systemic viral infection and better understand the interplay between
283 CD8 T cells and endothelial cells. C57BL/6 F2r$^{fl/fl}$ mouse carrying floxed Exon 2 of *F2r* gene was
284 conditionally targeted as well as fused in frame with p2A-Tomato (tdT) reporter cassette (as
285 described in Material and Methods section and Figure S1A).

286 C57BL/6 F2r$^{fl/fl}$ mice showed similar cell numbers in lymph nodes and spleen compared with
287 the wild type C57BL/6 (Figure S1B). The frequencies and cell count of innate cells including
288 neutrophils, eosinophils, monocytes, macrophages and dendritic cell subsets were similar between
289 the C57BL/6 F2r$^{fl/fl}$ and the C57BL/6 wild type mice (Figure S1C and D). Similarly, no significant
290 differences between C57BL/6 F2r$^{fl/fl}$ and wild type mice were observed in the frequencies and cell
291 numbers of lymphocytes subsets, B, NK and T cells in lymphoid organs (Figure S1E).

292 We next examine PAR1 expression by determining the frequency of tdTomato^{+} (tdT^{+}) cells,
293 immune cells. TdTomato was found in CD4 and CD8 T cells and NK cells but not in B cells
294 (Figure 1A, B and C). Similar to our previous observations in human T cells, CD8 T cells expressed

295 higher levels of PAR1 compared with CD4 T cells. Among lymphocytes, NK expressed the highest
296 level of PAR1 under steady state conditions (Figure 1C) (33).

297 mRNA of *F2r* expression in tdT expressing cells was further confirmed by qPCR in magnetic
298 cell isolated CD4 T cells, CD8 T cells and B cells. CD8 T cells expressed higher levels of mRNA
299 of *F2r* than CD4 T cells (Figure 1D). PAR1 protein expression in CD4 and CD8 T cells was further
300 confirmed by flow cytometry in tdT^+ T cells (Figure S2). These data show that under steady state
301 conditions, PAR1 is expressed in T and NK cells but not B cells.

302 We next investigated the expression of PAR1 in virus-specific CD8 T cells during a systemic
303 acute viral infection with the lymphocytic choriomeningitis virus Armstrong strain (LCMVArm).
304 This infection model recapitulates features of human viral infections, the acute form, LCMV
305 Armstrong (Arm) is cleared acutely at 8-10 days post infection (p.i) and induces the generation of
306 LCMV-specific memory CD8 T cells (59-61). LCMV is a non-cytolytic virus therefore the
307 pathology observed in infected hosts is mediated by the host immune response (62, 63).

308 Using this model, we aimed to study the inflammation mediated endothelial injury in the lung,
309 and address whether T cells are involved in endothelial repair after viral control. We studied two
310 time points post-infection: day 6 p.i (effector phase) and day 21 p.i (contraction phase and early
311 memory development) (61, 64). LCMVGp33-specific CD8 T cells secreted IFNγ, TNFα and
312 showed cytotoxic potential (as measured by CD107a surface expression) upon *in vitro* stimulation
313 with LCMVGp33-41aa peptide (Figure S3A and B). LCMVGp33-specific CD8 T cells peaked by
314 day 6 p.i in both the spleen and lung, then declined by day 21 in the spleen when the virus was
315 controlled (Figure S3A and B). In contrast, LCMVGp33-specific CD8 T cells in the lung, remained
316 elevated (Figure S3A and B).

317 Expression of PAR1 was monitored by tdT$^+$ cells in total CD8 T cells and virus-specific CD8
318 T cells using pentamer staining (H2-D^{b}LCMVGp33-41aa) (Figure S3C and Figure 1E
319 respectively). At day 6 p.i. and compared to total CD8 T cells from the naïve (dashed line) mice,
320 expression of PAR1 (tdT$^+$) in LCMVGp33-specific CD8 T cells was reduced, but was significantly
321 upregulated by day 21 p.i. (Figure 1E and F). Similar observations were noted in total CD8 T cells
322 in both spleen and lung (Figure S3C and 1E). PAR1 transcriptional regulation in LCMVGp33-
323 specific CD8 T cells may be induced by *in vivo* granzyme activation during degranulation (Figure
324 S3B) (33). Consistent with previous observations in degranulating human CD8 T cells, tdT
325 expression by CD107a$^+$CD8 T cells showed lower expression of granzyme A compared to
326 CD107a$^-$CD8 T cells (Figure S3E) (33). In addition, tdT$^+$CD8 T cells negatively correlated with
327 the frequency of GZMA$^+$CD8 T cells, R= -0.61, p= 0.02.
328 Altogether these data show that PAR1 is regulated at distinct stages of CD8 T cell activation,
329 with lower PAR1 expression at the effector phase and upregulated after viral control and memory
330 development.
331
332 **Angiogenic CD31^{high}CD8 T (T_{ang}) cells promote endothelial recovery during acute viral**
333 **infection**
334 In humans, T_{ang} cells were originally described in the center of endothelial progenitor cell
335 colonies isolated from peripheral mononuclear cells (PBMCs). In *in vivo* experiments, T_{ang} cells
336 support new vessel formation (25). However, whether T_{ang} cells are virus-specific CD8 T cells that
337 acquire these properties once the infection is controlled and are involved in endothelial repair
338 remains poorly understood. We hypothesized that systemic LCMVArm infection and its associated
339 inflammation induces endothelial injury in the lung, and T_{ang} cells play a role in repair after viral

340 control. We found at day 6 p.i., when LCMV-specific CD8 T cells are recruited into the lung, there
341 was a significant reduction in the frequency and cell count of lung endothelial cells (ECs) (Figure
342 1G). ECs recovered to baseline levels at day 21 p.i. (Figure 1G). In contrast to CD8 T cells,
343 expression of PAR1 in endothelial cells increased over the course of infection suggesting that
344 PAR1 can be targeted by different proteases during the course of the infection (Figure 1H). These
345 data show that a mild endothelial cell injury occurs in lung at the peak of CD8 T cell response and
346 recovers upon viral control.

347 We next determined if CD8 T cells are involved in the recovery of lung ECs. LCMV infected
348 mice were either treated with anti-CD8 mAb and IgG control at day 15 p.i. when the infection is
349 controlled. CD8 T cells were efficiently depleted in the lung by day 21 p.i. (Figure 2A). Compared
350 to the mice treated with IgG control, CD8 T cell depleted mice showed a delayed recovery of EC
351 count suggesting that CD8 T cells are involved in this process (Figure 2B). At this time point of
352 infection, we did not detect LCMV glycoprotein by qPCR in both spleen and lung suggesting viral
353 control (Figure S4A) (65).

354 We next tested the hypothesis that the delayed recovery of lung ECs is associated with the loss
355 of CD8 T_{ang} cells during depletion. T_{ang} cells have been defined by expression of CD31 (25). In
356 the lung, during the course of the LCMV infection, a small subset of CD8 T cells expressed
357 $CD31^{high}$ and CD309 (vascular endothelial growth factor receptor 2 (VEGFR2)) and although the
358 frequency showed an increased trend by day 21 p.i., it did not rich statistical significance (Figure
359 2C). In contrast, the number of $CD31^{high}$CD8 T cells was significantly increased at day 6 and 21
360 demonstrating an expansion of this subset during the recovery phase of lung ECs (Figure 2C). In
361 addition, similar PAR1 expression was observed in both $CD31^{high}$ and $CD31^{low}$ CD8 T cells
362 (Figure S4B).

363 We then investigated whether CD31^{high}CD8 T cells were LCMV-specific and secrete
364 cytokines upon *in vitro* stimulation with LCMVGp33 peptide (Figure 2D). At day 21 p.i. and
365 compared to CD31^{neg}CD8 T cells, CD31^{high}CD8 T_{ang} cells secrete similar levels of IFNγ, TNFα
366 and have similar cytotoxic potential (CD107a). Of note, the frequency of CD31^{high}LCMVGp33-
367 specific CD8 T cells single IFNγ producers were reduced compared to the CD31^{neg} (Figure 3D).
368 Interestingly, LCMVGp33-specific CD31^{high}CD8 T cells were enriched in the memory
369 precursor effector T cells (KLRG1^{-}CD127^{+}), which have survival advantage during the
370 contraction phase and possesses plasticity to give rise to multiple memory subsets (Figure 2E)
371 (66-69). As expected, at day 21 p.i., a reduction of double positive effectors (KLRG1^{+}CD127^{+})
372 and short-live effector KLRG1^{+}CD127^{-} and KLRG1^{-}CD127^{-} CD8 T cells was observed at day
373 21 p.i. (Figure 2E).
374 In addition, we evaluated the ability of lung CD31^{high}CD8 T cells to secrete pro-angiogenic
375 cytokines and T cell helper cytokines. We sorted CD31^{high} and CD31^{neg} bulk CD8 T cells from
376 lung of LCMV mice infected at day 21 p.i., and CD31^{high} bulk CD8 T cells from lung of naïve
377 mice as control. Sorted subsets were TCR stimulated with cross-linked CD3 and CD28 mAbs for
378 3 days and cytokines were measured in the supernatants (Figure 2F and Figure S4C). CD31^{high}
379 but not CD31^{neg}CD8 T cells secreted vascular endothelial growth factor (VEGF), a cytokine that
380 induces proliferation of ECs suggesting a pro-angiogenic function (70, 71). In addition, both
381 CD31^{neg} and CD31^{high}CD8 T cells showed similar ability to secrete granulocyte-macrophage-
382 colony stimulating factor (GM-CSF), known to induce EC proliferation and mobilize endothelial
383 progenitor cells from the bone marrow (Figure S4C) (72, 73). Lastly, CD31^{high}CD8 T cells showed
384 the ability to secrete of IL-2 and secrete low levels of Th2, Th17, Th22 and Th9 associated
385 cytokines (Figure S4C).

386 These data suggest that angiogenic CD31^{high}CD8 T_{ang} cells are virus specific with an enriched
387 memory precursor phenotype. CD31^{high}CD8 T_{ang} secrete VEGF suggesting may contribute with
388 lung EC recovery after viral control.
389
390 **Endothelial recovery is associated to CD31^{high}CD8 T_{ang} cells**
391 We next investigated the relationships between CD8 T_{ang} cells and lung ECs during the course
392 of the LCMV infection. ECs are heterogenous and play important roles by supporting immune cell
393 trafficking and regulating inflammation during immunity (74-76). Diverse phenotypes with
394 distinct functions including "immune cell-like" and "developmental/regenerative" involved in
395 immunity and repair respectively have been described (77, 78).
396 We hypothesized that during the phase of CD31^{high}CD8 T_{ang} cells expansion and EC recover,
397 ECs would be enriched with a regenerative phenotype. We determined the expression of markers
398 associated with inflammation (PD-L1, VCAM1) and proangiogenic/repair (CD34, CD309,
399 CD105) (63, 77, 79, 80). CD309 is a receptor for the VEGF, an essential factor for EC function
400 during angiogenesis (70). CD105 (Endoglin) binds to different components of the TGF-β
401 superfamily and also regulates endothelial proliferation, migration, and vascular homeostasis (81,
402 82). In addition, CD90.2 was used as maker for lymphatic endothelial cells (83).
403 We performed an unsupervised cluster analysis using PhenoGraph to classify high-parameter
404 single-cell data into phenotypically distinct clusters (84). We concatenated 10,000 events per
405 mouse of CD326^{-}CD45^{-}CD31^{+} lung ECs from naïve and LCMV infected mice from day 6 and 21
406 p.i. to analyze changes in endothelial cells (Figure 3A).
407 We found that the frequency of lung EC clusters (CL) 1, 2, 3, and small CL 7, and 8
408 significantly increased at day 6.p.i (Figure 3A, bubble plots and Figure S5). These CLs expressed

409 higher levels of PD-L1 and distinct levels of CD31 and PAR1 (Figure 3A). Expression of PD-L1
410 suggest that endothelial cells interact with immune cells regulating their function and potential
411 immune mediated pathology through PD1-PD-L1 interaction (85).

412 The CL4, 5, 6, and 13 were present in the naïve mice and at day 21 p.i. (Figure 3A and Figure
413 S5). These clusters expressed markers associated with EC proliferation including CD105
414 (Endoglin), and CD309 (VEGFR2), A small EC subset (CL14), expressed high levels of CD105
415 and was expanded by day 21 p.i. suggesting a "regenerative" phenotype (Figure S5). In addition,
416 CL10 and CL11 remained significantly reduced compared to the naïve mice. CL9 correspond to
417 CD90.2^{+} lymphatic endothelial cells and its frequency remained constant through the course of the
418 infection.

419 These data suggested that ECs are heterogenous and dynamic during a viral infection. The ECs
420 in CL6 expressed CD201 (endothelial protein C receptor, EPCR), a marker associated with
421 resident vascular endothelial cell progenitors and activated protein C (APC) dependent activation
422 of PAR1 during angiogenesis (78, 86, 87). Importantly, CL6 expressed higher levels of CD105,
423 CD309 and CD34 suggesting a proliferative and regenerative phenotype (79). Moreover, CL6 was
424 positively associated (R= 0.66, p< 0.01) with the frequency of CD31^{high}CD8 T_{ang} cells suggesting
425 a potential interaction during vascular remodeling (Figure 3B).

426 Altogether these data suggest that CD31^{high}CD8 T_{ang} cells may play a role in endothelial
427 recovery by secreting VEGF promoting proliferation of endothelial cells.

428

429 **Circulating angiogenic CD8 T (T_{ang}) cells from PWH have proinflammatory phenotype.**

430 In humans with chronic inflammatory diseases reduced frequencies of T_{ang} cells are associated
431 with cardiovascular risk (25, 28, 29). The role of T_{ang} cells in the setting of human chronic viral

432 infections such as HIV remains to be defined. Previously, we reported that circulating T_{ang} cells
433 from PWH express the vascular homing receptor CX3CR1 suggesting their recruitment to the sites
434 of endothelial inflammation (88). Given that T cell immune activation and systemic inflammation
435 are the main features of chronic HIV infection, we hypothesized that this environment alters T_{ang}
436 cell function promoting a proinflammatory function that contributes to endothelial inflammation.
437 To address this question, we investigated circulating T_{ang} cells in PBMCs from PWH (n= 25) and
438 uninfected controls people without HIV (PWoH, n=17). PWH had a median CD4 count 663 (532-
439 861.5) cells/μL and HIV RNA viral load < 20 copies/mL (n= 20) and 50-110 copies/mL (n= 4).
440 Study participants had a median ASCVD (Atherosclerosis Cardiovascular Disease) risk score of
441 7.9 (IQR: 5.0-18.6) (Table 1).

442 In humans, T_{ang} cells are defined as surface expression of CD31/PECAM-1 (Platelet
443 Endothelial Cell Adhesion Molecule) and the chemokine receptor CXCR4 (receptor for the
444 Stromal Cell Derived Factor-1) *(25, 89)*. Flow cytometric analysis showed that in PWH there is a
445 significantly reduction in the frequencies of circulating CD8 T_{ang} cells ($p < 0.001$). A trend,
446 although not statistically significant was observed in CD4 T_{ang} cells as well (Figure 4A and B).

447 To evaluate the impact of HIV driven immune activation, we studied expression of markers
448 associated with adhesion, homing and trafficking during vascular inflammation including the
449 PAR1 (30, 31, 33). We investigated the vascular homing receptor CX3CR1 that binds to CX3CL1
450 (fractalkine) expressed by inflamed endothelial cells, and the integrin CD49f (Integrin alpha-6)
451 that binds to laminin, a component of the vascular basement membrane (30-32, 90). In PWH, both
452 CD4 T_{ang} and CD8 T_{ang} cells showed significantly increased expression of PAR1, CX3CR1 and
453 CD49f compared to PWoH suggesting an increased potential for recruitment and trafficking to the
454 sites of vascular inflammation (Figure 4C and D). In addition to the increased trafficking potential,

455 both CD4 T_{ang} and CD8 T_{ang} cells from PWH showed an increased expression of effector
456 molecules Granzyme A (GZMA) and Granzyme B (GZMB) when compared to PWoH (Figure
457 4E).

458 All together these data suggest that PWH and virally suppressed by ART have a significant
459 reduction in the frequencies of CD8 but not CD4 T_{ang} cells. T_{ang} cells showed a differentiated
460 phenotype with cytotoxic potential and increased potential to migrate to the sites of vascular
461 inflammation.

462

463 **Frequencies of activated CD8 T_{ang} cells are associated with cardiovascular risk in PWH**

464 In PWH, immune activation, systemic inflammation and endothelial dysfunction have been
465 identified as the main drivers of cardiovascular events (3, 5, 6, 16). The data above suggest that in
466 the context of HIV infection T_{ang} cells have a proinflammatory phenotype. We next investigated
467 the relationship between activation markers expressed by T_{ang} cells and the Atherosclerotic
468 Cardiovascular Disease (ASCVD) risk score (Figure 4F, G and H).

469 The frequencies of circulating total CD4 and CD8 T_{ang} cells did not show an association with
470 ASCVD. In contrast, we observed a positive correlation between ASCVD and the frequency of
471 cells expressing activation markers including homing and trafficking $CX3CR1^{+}PAR1^{+}$CD8 T_{ang}
472 and $CD49f^{+}PAR1^{+}$CD8 T_{ang} (R= 0.50, p= 0.04 and R= 0.58, p= 0.02 respectively) (Figure 4F and
473 G). Similarly, $GZMA^{+}GZMB^{+}$CD8 T_{ang} cells showed a positive association with the ASCVD risk
474 score R= 0.65, p< 0.01 (Figure 4H). Of note is that expression of these markers in CD4 T_{angs} cells
475 did not correlate with ASCVD risk (Figure 4F, G and H). These observations suggest that in PWH
476 immune activation of CD8 T_{ang} cells drives a proinflammatory phenotype and may play a role in
477 sustaining endothelial inflammation.

478 To better address the potential contribution of activated CD8 T_{ang} cells on endothelial
479 inflammation, we further studied the relationship between plasma levels of biomarkers of
480 endothelial inflammation and immune cell trafficking including soluble Vascular and Intracellular
481 Adhesion Molecule-1 (sVCAM-1 and sICAM-1 respectively), IL-6; and T cell-derived cytokines
482 and effector molecules including TNFα, IFNγ, IL-2, sFASL, GZMA and GZMB (Figure 4I and
483 Figure S6A). We found that plasma levels of GZMA but not GZMB were positively associated
484 with IL-6 (R= 0.62, p< 0.001). sVCAM-1 showed a positive trend (R= 0.449, *p*= 0.024) but not
485 with sICAM-1 (Figure 4I). As expected, plasma levels of cytokines (TNFα, IFNγ, sFASL, IL-2)
486 positively correlated with the plasma levels of granzymes (Figure S6A).
487 Altogether the data shows that chronic HIV driven immune activation increase trafficking and
488 proinflammatory properties of CD8 T_{ang} cells. Moreover, the association with ASCVD suggest
489 that CD8 T_{ang} cells may contribute to endothelial inflammation, dysfunction and disease risk.
490
491 ***In vitro,* CD8 T_{ang} cells from PWH showed enhanced ability to induced sICAM-1 and**
492 **VCAM-1 by endothelial cells.**
493 The above results suggest that chronic HIV infection alters CD8 T_{ang} cells skewing their
494 function to pro-inflammatory. Because activated CD8 but not CD4 T_{ang} cells showed association
495 with cardiovascular risk, in the following sections of the manuscript we focused our study on CD8
496 T_{ang} cells. To address the potential mechanisms involved by which CD8 T_{ang} cells drive endothelial
497 inflammation, we first determined the effects of *in vitro* activated CD8 T_{ang} cells on primary human
498 umbilical vein endothelial cells (HUVEC). In the supernatants of the co-cultures, we measured
499 adhesion molecules including sICAM-1 and sVCAM-1, proinflammatory cytokines IL-6,

500 angiopoetin-2 (Ang-2) and IL-8 (CXCL8); and pro-angiogenic cytokines, basic Fibroblast Growth
501 Factor (bFGF) and Vascular Endothelial Growth Factors (VEGF) (91-93).

502 CD8 T_{ang} cells from PWH (n= 10) and PWoH (n= 10) were sorted based on the expression of
503 CD31, CXCR4 and memory phenotype. CD8 T_{ang} cells were *in vitro* expanded with anti-
504 CD3/CD28 mAbs and rhIL-2 (50 U/ml) for 14 days. Expanded CD8 T_{ang} cells were co-cultured
505 with HUVEC at 20:1 CD8 T_{ang} to HUVEC ratio and stimulated in media (control) and with anti-
506 CD3/CD28 mAbs coated beads overnight.

507 CD8 T_{ang} co-cultured with HUVEC cells in media alone showed negligible levels of shedding
508 of sICAM-1 and sVCAM-1. In contrast, when CD8 T_{ang} cells were TCR stimulated a significant
509 increase of sICAM-1 and sVCAM-1 was detected in the supernatant of the cultures (Figure 5A).
510 The effects mediated by CD8 T_{ang} cells from PWH were significantly higher than those observed
511 with CD8 T_{ang} cells from PWoH (Figure 5A). Moreover, stimulation of CD8 T_{ang} from PWH led
512 to an increased trend, although did not reach statistical significance, in the production of
513 proinflammatory and pro-angiogenic cytokines IL-6, and bFGF respectively. No differences were
514 observed in the secretion of IL-8, Ang-2 or VEGF. (Figure 5B). The combination of cytokines
515 IFNγ (10 ng/mL) and TNFα (0.5 ng/mL) used as positive control in HUVEC cultured alone,
516 showed no statistically significant effect on the shedding of sVCAM-1, sICAM-1. In addition, low
517 IL-6 secretion was observed suggesting that CD8 T_{ang} cell-HUVEC contact dependent mechanism
518 is involved in mediating shedding of adhesion molecules and IL-6 secretion by endothelial cells
519 (Figure S6B and Figure 5B). Similar levels of Ang-2, IL-8/CXCL8 and the pro-angiogenic
520 cytokines VEGF and FGFb were detected when endothelial cells were stimulated with
521 combination IFNγ and TNFα (Figure S6B).

522 These observations suggest that secretion of cytokines and effector molecules from activated
523 CD8 T_{ang} cells can lead to endothelial activation promoting trafficking of immune cells and
524 secretion of proinflammatory and pro-angiogenic cytokines by endothelial cells.

525 We next performed a tube forming assay in which endothelial cells cultured in an extracellular
526 matrix form capillary-like structures as a measurement of angiogenesis to better evaluate the
527 interactions between CD8 T_{ang}-endothelial cells (94). CD8 T_{angs} cells were sorted from PBMCs,
528 labeled with CFSE and cultured with HUVEC at 1:2 T cell to HUVEC ratio (Figure 5C and D).

529 CD8 T_{ang} cells overtime migrate and adhere to the endothelial cells as the tubes formed
530 showing a mesh of capillary-like structures and $CFSE^{+}$CD8 T_{ang}, suggesting a close interaction
531 with endothelial cells in the extracellular matrix (Figure 5C and D). Overtime, $CSFE^{+}$CD8 T_{ang}
532 from PWH and sorted HIV_{Gag} specific CD8 T cells showed a trend of slowing the growth of the
533 tube (loop area), although these responses were heterogenous among the donors (Figure 5E). In
534 contrast, CD8 T_{ang} from PWoH showed a trend promoting bigger loop area overtime.

535 Altogether, these data imply a crosstalk between CD8 T_{ang} cells and endothelial cells. CD8
536 T_{ang} cells from PWH promote endothelial activation (ICAM1 and VCAM1), and induced secretion
537 of proinflammatory and pro-angiogenic cytokines influencing endothelial cell function.

538

539 **Activated CD8 T_{ang} cells mediate endothelial cell activation through a granzyme-**
540 **dependent PAR1 activation**

541 We next investigated the mechanisms by which CD8 T_{ang} cells activate endothelial cells.
542 PAR1 is expressed by endothelial cells and its signaling mediates important functions in
543 maintaining barrier function (35). In addition to thrombin, PAR1 is activated by other proteases
544 including extracellular granzymes (A, B and K) regulating angiogenesis and extracellular

545 remodeling (51-53). These observations led us to the hypothesis that granzymes are involved in
546 endothelial activation in the context of HIV infection.

547 We next studied the effects of granzymes in endothelial cells. To isolate the effects of
548 granzymes from cytokines secreted by CD8 T_{ang} cells we used recombinant human (rh) GZMA
549 and GZMK. GZMA and GZMK have tryptase activity and preferentially cleave after basic
550 residues (Arg and Lys) which is similar to thrombin. GZMB is an aspartase and cleaves after Asp
551 (48, 49, 54, 55).

552 We determined the effects of GZs dependent PAR1 activation on calcium mobilization.
553 HUVEC were cultured *in vitro* and activated either with rhGZMA (100nM) and Thrombin (3nM).
554 Compared to thrombin, GZMA induced a calcium mobilization with slower kinetics and sustained
555 overtime (Figure 6B). These effects were not observed on GZMK and GZMB. We then
556 investigated the downstream effects induced by GZM-dependent activation of PAR1 at later time
557 points of stimulation and measure cytokine secretion by endothelial cells (Figure 6C).

558 HUVEC were activated with either rhGZMA and rhGZMK (100 nM) in the absence or
559 presence of PAR1 antagonist SCH530348 which inhibit binding of the tethered ligand (Figure 6A).
560 In addition, we used the mAb ATAP-2 that blocks PAR1 cleavage by binding to an epitope within
561 the PAR1 tethered ligand domain, Figure 6A (42, 95-97). As positive control, we used an agonist
562 peptide specific for PAR1 (mimics the tethered ligand) and mediates activation of PAR1 in a
563 cleavage independent manner (Figure 6A).

564 We found that rhGZMA and rhGZMK induced secretion of proinflammatory cytokines IL-6,
565 IL-8/CXCL8 and Ang-2 (Figure 6 and Figure S6C). Moreover, GZA and GZK induced pro-
566 angiogenic cytokine VEGF, albeit at lower levels (Figure S7). The antagonist SCH530348
567 (vorapaxar) partially blocked PAR1 activation by rhGZMA and consequently the secretion of IL-

568 6 and IL-8 and Ang-2 (Figure 6C, D and E). The effects mediated by the ATAP-2 mAb showed
569 inhibition Ang-2 but not IL-6 and IL-8.

570 In addition, rhGZMK dependent PAR1 activation by the antagonist SCH530348 inhibited
571 secretion of IL-6 and IL-8/CXCL8 but not Ang-2 secretion by endothelial cells (Figure 6C, D and
572 E). In contrast, ATAP-2 mAb blocked GZMK dependent PAR1 activation and the secretion of
573 IL-6, IL-8/CXCL8 and Ang-2 (Figure 6C and S7). As expected, stimulation with PAR1 agonist
574 peptide (cleavage independent activation) induced secretion of IL-6 and IL-8, however it did not
575 induce a significant increase in secretion of Ang-2 (Figure 6H and S6C).

576 All together these data suggest that CD8 T_{ang} cells mediate endothelial cell activation in part
577 through GZMA and GZMK dependent PAR1 activation leading to the secretion of
578 proinflammatory cytokines.

579

580 **Discussion**

581 Chronic CD8 T cell activation is associated with increased cardiovascular disease risk in PWH,
582 however the mechanisms remain to be defined (6, 10, 16, 18, 22). Because endothelial
583 inflammation and dysfunction are the main features of cardiovascular disease, in the present study
584 we investigated a physiological mechanism in which the immune system (with a focus on CD8 T
585 cells) intersects with vascular repair. PAR1 connects the coagulation cascade, endothelial cells and
586 CD8 T cells at the site of vascular injury, in this study, using a PAR1 reporter mouse we established
587 the kinetics of PAR1 expression in virus-specific CD8 T cells during the course of an acute viral
588 infection with LCMV. PAR1 expression in LCMV-specific CD8 T cells is downregulated during
589 the effector phase and its expression is upregulated during the contraction phase and early memory
590 development (day 21 p.i). In addition, we identified a subset of $CD31^{high}$CD8 T cells that secrete
591 VEGF providing evidence that CD8 T_{ang} cells may contributes to vascular repair after viral control.

592 T_{ang} cells were originally discovered in the center of endothelial progenitor cell colonies from
593 PBMCs by Hur J. et al. (25-27). However, whether T_{ang} cells play a role during infection is not
594 well understood. We found that expansion of $CD31^{high}$CD8 T_{ang} cells occurs concomitant with the
595 EC recovery and secrete proangiogenic cytokines VEGF and GMCSF. These cytokines are
596 associated with endothelial cell proliferation, survival and bone marrow mobilization of
597 endothelial progenitors (70-72, 98). Our study shows that $CD31^{high}$CD8 T_{ang} cells may regulate
598 angiogenesis by promoting the recruitment of endothelial progenitor cells, and other cells
599 including myeloid cells to the site of vascular injury.

600 Particularly, $CD31^{high}$CD8 T_{ang} cells expressed CD309 (VEGFR2) and secrete proangiogenic
601 and Th1 cytokines. Similar to these findings, a study reported that hypoxia upregulates expression
602 of CD309 (VEGFR2) and VEGF signaling, which in turn increased expression of IFNγ and

603 inhibited IL-10 (71). In our model of LCMV infection, there is a mild endothelial injury that may
604 induce hypoxia driving expression of CD309 and secretion of VEGF by CD8 T_{ang} cells. It is also
605 possible VEGF signal promotes the acquisition of a proangiogenic property by CD8 T_{ang} cells and
606 warrants further investigation.

607 CD8 T cells are predominantly viewed as main players in immunity against viruses and cancer
608 due to their cytotoxic function, however, emerging evidence suggest that they play a role in tissue
609 regeneration and remodeling. $CD31^{high}$CD8 T_{ang} cells were LCMV-specific and secrete VEGF,
610 IFNγ and TNFα and degranulate upon *in vitro* stimulation LCMVGp33 suggesting may acquire
611 this function after viral control. More importantly, $CD31^{high}$CD8 T_{ang} cells showed a memory
612 precursor phenotype ($KLGRG1^{-}CD127^{+}$) suggesting a survival advantage during the contraction
613 phase and a proliferative potential (66-69).

614 Expression of CD31 in T cells has been associated with T cell trafficking and studies have
615 shown that CD31 attenuates TCR signaling in T cells as contains two immunoreceptor tyrosine-
616 based inhibitory motif (ITIM) units in the cytoplasmic domain (99-101). It is possible that CD31
617 expression by CD8 T_{ang} cells allows close interactions with endothelial cells preventing their
618 potential cytotoxic activity on endothelial cells. CD8 T cells with tissue remodeling properties that
619 secrete IFNγ, TNFα and epidermal growth factor receptor (EGFR)-ligand amphiregulin (AREG)
620 have been described highlighting CD8 T cell function beyond cytotoxicity (102). Moreover, in
621 pathological conditions such as retinal vascular diseases, VEGF producing CD8 T cells drive
622 inflammation and abnormal angiogenesis suggesting that dysregulated T_{ang} cell function may
623 contribute to the pathology of disease (103).

624 We also investigated changes in lung endothelial cells. ECs are heterogenous and play distinct
625 roles during immune response by supporting trafficking of immune cells, immune functions

626 (immune cell-like ECs) and repair (regenerative ECs) (76, 104). Particularly, our study shows that
627 at the peak of CD8 T cell recruitment into the lung, ECs expressed high levels of PD-L1 likely
628 induced by cytokines produced by LCMV-specific CD8 T cells regulating the immune mediated-
629 pathology including endothelial injury (105). The "immune-EC" phenotype returns to basal levels
630 when the virus is controlled and ECs expressing receptors associated with cell proliferation and
631 survival (CD34, CD309, CD105, CD201) are more predominant. Studies of lung endothelial cells
632 in response to acute lung injury by LPS and influenza infection using single cell RNAseq, revealed
633 distinct functions of ECs "immune-ECs" and "regenerative- ECs" the later involved in vascular
634 remodeling suggesting an important cross-talk between ECs, host immunity and endothelial repair
635 (77, 79). In contrast to these studies that used an acute respiratory lung viral infection or injury,
636 we used a systemic virus to evaluate vascular injury and investigate potential mechanisms
637 associated with chronic HIV infection and endothelial inflammation. Similar to our studies, the
638 authors observed a trend of reduced EC count at day 7 p.i, (79). Although this study did not
639 investigate the potential mechanisms driving proliferation of ECs in the reconstitution phase
640 (between day 14 to 21 p.i), they described a proliferating population of $CD34^{+}$ECs with
641 regenerative capacity (79). We found that CD8 T_{ang} cells are associated with population of ECs
642 (cluster 6) that express CD34 and have the potential to proliferate in response to proangiogenic
643 cytokines through CD309 and CD105 signaling. CD309, the receptor for VEGF, is a critical factor
644 for endothelial cell proliferation, migration, and survival, and plays important role during vascular
645 remodeling (106). In addition, CD105, a marker for endothelial cell proliferation, is expressed on
646 vascular endothelium during angiogenesis and prevents endothelial cell apoptosis induced by
647 TGFβ (107). Moreover, this EC population express of endothelial protein C receptor (CD201) that

648 has been proposed as a marker of endothelial progenitor cells with new vessel forming properties
649 (86, 108).

650 T_{ang} cells are key players in maintaining endothelial homeostasis and alterations in vascular
651 repair mechanisms may contribute to endothelial dysfunction and increase cardiovascular disease
652 risk (109). In fact, reduced proportion of circulating T_{angs} has been associated with age and
653 increased cardiovascular risk (25, 28, 29). Patients with rheumatoid arthritis and inflammatory
654 diseases that suffered a cardiovascular event complication had lower circulating T_{ang} cells (29, 89,
655 110-114). In this study, we found that compared with uninfected controls (PWoH), CD8 T_{ang} cells
656 from PWH had proinflammatory phenotype, express PAR1, and the adhesion and homing
657 receptors CD49f and CX3CR1 respectively (32, 90, 115). In addition, CD8 T_{ang} cells had cytotoxic
658 potential and expressed GZMA and GZMB. The activated phenotype of CD8 T_{ang} cells but not
659 CD4 T_{ang} was associated with the ASCVD suggesting a relationship between endothelial
660 inflammation and CD8 T_{ang} cell immune activation.

661 Granzymes (GZMA, GZMB, GZMK), can activate PAR1 and induce a "biased" or non-
662 canonical signal distinct from thrombin (51, 116, 117). GZMs were first thought to be involved
663 in cytotoxic function and recent evidence suggests non-cytotoxic and extracellular biological
664 activities including regulation of vascular integrity, angiogenesis, extracellular matrix remodeling
665 and trans-endothelial migration (45-47, 49, 51-53, 116, 118). The present study shows that, *in*
666 *vitro*, CD8 T_{ang} cells induced activation of ECs via granzyme induced production of
667 proinflammatory cytokines. In addition, granzyme dependent PAR1 activation provides a potential
668 mechanism by which HIV alters proangiogenic function and the chronic stimulation of this
669 pathway may lead endothelial inflammation and dysfunction.

670 Granzymes are emerging as potential contributors of inflammation in cardiovascular diseases
671 (51, 116, 119, 120). Recent study reported a subset of CD8 T cells expression GZMK and GZMB
672 with proinflammatory (rather than cytotoxic) function in chronically inflamed human tissues
673 supporting their potential role in inflammation (53). Moreoever, increased levels of GZMs in
674 biological fluids and tissues has been reported in inflammatory conditions including cardiovascular
675 disease, autoimmunity, chronic obstructive pulmonary disease, and cancer (51, 53, 121, 122).
676 Supporting these observations, we found an association between plasma GZMA leves and
677 endothelial inflammation markers including sVCAM1 and IL-6 was observed in PWH suggesting
678 that ongoing endothelial inflammation in the setting of suppressed viremia may be driven by T_{ang}
679 cell activation.

680 Alltoghether these data highlight a novel role of CD8 T_{ang} cells in vascular remodeling, and
681 granzyme-PAR1 dependent pathway promoting endothelial inglammation. CD8 T_{ang} cells and
682 GZMA dependent PAR1 activation could be a target of intervetion to reduce endothelial
683 inflammation and injury in PWH potentially mitigating the risk of cardiovascular disease during
684 chronic HIV infection.

Acknowledgements

Research reported in this publication was supported by the National Institute of Allergy and Infectious Diseases of the National Institutes of Health under award number NIH R01AI145549 and R21AI186960. We thank the District of Columbia Center for AIDS Research, an NIH funded program (P30AI117970) which is supported by the following NIH Co-Funding and Participating Institutes and Centers: NIAID, NCI, NICHD, NHLBI, NIDA, NIMH, NIA, NIDDK, NIMHD, NIDCR, NINR, FIC and OAR. The content of this publication does not necessarily reflect the views or policies of the Department of Health and Human Services, nor does mention of trade names, commercial products, or organizations imply endorsement by the U.S. Government.

Authors' contributions

MC conceptualized the study and supervise data analysis. TL, CM, CJ performed and analyzed mice experiments, JC, ZZ, MFC, MA, SY, performed human experiments, JK, PK, HC recruited patients, KDV, GPA advise and performed endothelial assay, DBG and LP advice mice infection model. MC, TL and LP wrote the manuscript.

701 **References**

702 1. Baker JV, Sharma S, Grund B, Rupert A, Metcalf JA, Schechter M, et al. Systemic
703 Inflammation, Coagulation, and Clinical Risk in the START Trial. *Open Forum Infect*
704 *Dis.* 2017;4(4):ofx262.
705 2. Hadigan C, Paules CI, and Fauci AS. Association Between Human Immunodeficiency
706 Virus Infection and Cardiovascular Diseases: Finding a Solution to Double Jeopardy.
707 *JAMA Cardiol.* 2017;2(2):123-4.
708 3. Hsue PY, Deeks SG, and Hunt PW. Immunologic basis of cardiovascular disease in HIV-
709 infected adults. *The Journal of infectious diseases.* 2012;205 Suppl 3:S375-82.
710 4. Sinha A, Ma Y, Scherzer R, Hur S, Li D, Ganz P, et al. Role of T-Cell Dysfunction,
711 Inflammation, and Coagulation in Microvascular Disease in HIV. *Journal of the*
712 *American Heart Association.* 2016;5(12).
713 5. Freiberg MS, Chang CC, Kuller LH, Skanderson M, Lowy E, Kraemer KL, et al. HIV
714 infection and the risk of acute myocardial infarction. *JAMA internal medicine.*
715 2013;173(8):614-22.
716 6. Mattingly AS, Unsal AB, Purdy JB, Gharib AM, Rupert A, Kovacs JA, et al. T-cell
717 Activation and E-selectin Are Associated With Coronary Plaque in HIV-infected Young
718 Adults. *The Pediatric infectious disease journal.* 2017;36(1):63-5.
719 7. Serrano-Villar S, Sainz T, Lee SA, Hunt PW, Sinclair E, Shacklett BL, et al. HIV-
720 infected individuals with low CD4/CD8 ratio despite effective antiretroviral therapy
721 exhibit altered T cell subsets, heightened CD8+ T cell activation, and increased risk of
722 non-AIDS morbidity and mortality. *PLoS Pathog.* 2014;10(5):e1004078.
723 8. Stein JH, and Hsue PY. Inflammation, immune activation, and CVD risk in individuals
724 with HIV infection. *JAMA.* 2012;308(4):405-6.
725 9. Triant VA, Perez J, Regan S, Massaro JM, Meigs JB, Grinspoon SK, et al.
726 Cardiovascular Risk Prediction Functions Underestimate Risk in HIV Infection.
727 *Circulation.* 2018;137(21):2203-14.
728 10. Shah ASV, Stelzle D, Lee KK, Beck EJ, Alam S, Clifford S, et al. Global Burden of
729 Atherosclerotic Cardiovascular Disease in People Living With HIV: Systematic Review
730 and Meta-Analysis. *Circulation.* 2018;138(11):1100-12.
731 11. Lundgren JD, Babiker AG, Sharma S, Grund B, Phillips AN, Matthews G, et al. Long-
732 Term Benefits from Early Antiretroviral Therapy Initiation in HIV Infection. *NEJM Evid.*
733 2023;2(3).
734 12. Catalfamo M, Wilhelm C, Tcheung L, Proschan M, Friesen T, Park JH, et al. CD4 and
735 CD8 T cell immune activation during chronic HIV infection: roles of homeostasis, HIV,
736 type I IFN, and IL-7. *J Immunol.* 2011;186(4):2106-16.
737 13. Nou E, Lo J, and Grinspoon SK. Inflammation, immune activation, and cardiovascular
738 disease in HIV. *AIDS (London, England).* 2016;30(10):1495-509.
739 14. Imamichi H, Smith M, Adelsberger JW, Izumi T, Scrimieri F, Sherman BT, et al.
740 Defective HIV-1 proviruses produce viral proteins. *Proceedings of the National Academy*
741 *of Sciences of the United States of America.* 2020;117(7):3704-10.
742 15. Benlarbi M, Richard J, Bourassa C, Tolbert WD, Chartrand-Lefebvre C, Gendron-Lepage
743 G, et al. Plasmatic HIV-1 soluble gp120 is associated with correlates of immune
744 dysfunction and inflammation in ART-treated individuals with undetectable viremia. *The*
745 *Journal of infectious diseases.* 2023.

746 16. Longenecker CT, Funderburg NT, Jiang Y, Debanne S, Storer N, Labbato DE, et al.
747 Markers of inflammation and CD8 T-cell activation, but not monocyte activation, are
748 associated with subclinical carotid artery disease in HIV-infected individuals. *HIV Med.*
749 2013;14(6):385-90.
750 17. Hsue PY, Deeks SG, and Hunt PW. Immunologic basis of cardiovascular disease in HIV-
751 infected adults. *The Journal of infectious diseases.* 2012;205 Suppl 3(Suppl 3):S375-82.
752 18. Kaplan RC, Sinclair E, Landay AL, Lurain N, Sharrett AR, Gange SJ, et al. T cell
753 activation and senescence predict subclinical carotid artery disease in HIV-infected
754 women. *J Infect Dis.* 2011;203(4):452-63.
755 19. McLaughlin MM, Ma Y, Scherzer R, Rahalkar S, Martin JN, Mills C, et al. Association
756 of Viral Persistence and Atherosclerosis in Adults With Treated HIV Infection. *JAMA*
757 *Netw Open.* 2020;3(10):e2018099.
758 20. Turcotte I, El-Far M, Sadouni M, Chartrand-Lefebvre C, Filali-Mouhim A, Fromentin R,
759 et al. Association Between the Development of Subclinical Cardiovascular Disease and
760 Human Immunodeficiency Virus (HIV) Reservoir Markers in People With HIV on
761 Suppressive Antiretroviral Therapy. *Clin Infect Dis.* 2023;76(7):1318-21.
762 21. Wang Y, Brichacek B, Dubrovsky L, Pushkarsky T, Korolowicz K, Rodriguez O, et al.
763 Increased Atherosclerosis in HIV-Infected Humanized Mice Is Caused by a Single Viral
764 Protein, Nef. *The Journal of infectious diseases.* 2025;232(1):e116-e25.
765 22. Karim R, Mack WJ, Kono N, Tien PC, Anastos K, Lazar J, et al. T-cell activation, both
766 pre- and post-HAART levels, correlates with carotid artery stiffness over 6.5 years
767 among HIV-infected women in the WIHS. *J Acquir Immune Defic Syndr.*
768 2014;67(3):349-56.
769 23. Keller TT, Mairuhu AT, de Kruif MD, Klein SK, Gerdes VE, ten Cate H, et al. Infections
770 and endothelial cells. *Cardiovascular research.* 2003;60(1):40-8.
771 24. Wang Y, Brichacek B, Dubrovsky L, Pushkarsky T, Korolowicz K, Rodriguez O, et al.
772 Increased atherosclerosis in HIV-infected humanized mice is caused by a single viral
773 protein, Nef. *The Journal of infectious diseases.* 2025.
774 25. Hur J, Yang HM, Yoon CH, Lee CS, Park KW, Kim JH, et al. Identification of a novel
775 role of T cells in postnatal vasculogenesis: characterization of endothelial progenitor cell
776 colonies. *Circulation.* 2007;116(15):1671-82.
777 26. Asahara T, Murohara T, Sullivan A, Silver M, van der Zee R, Li T, et al. Isolation of
778 putative progenitor endothelial cells for angiogenesis. *Science (New York, NY.*
779 1997;275(5302):964-7.
780 27. Yoder MC. Endothelial stem and progenitor cells (stem cells): (2017 Grover Conference
781 Series). *Pulm Circ.* 2018;8(1):2045893217743950.
782 28. Rouhl RP, Mertens AE, van Oostenbrugge RJ, Damoiseaux JG, Debrus-Palmans LL,
783 Henskens LH, et al. Angiogenic T-cells and putative endothelial progenitor cells in
784 hypertension-related cerebral small vessel disease. *Stroke; a journal of cerebral*
785 *circulation.* 2012;43(1):256-8.
786 29. Rodriguez-Carrio J, Alperi-Lopez M, Lopez P, Alonso-Castro S, Ballina-Garcia FJ, and
787 Suarez A. Angiogenic T cells are decreased in rheumatoid arthritis patients. *Annals of the*
788 *rheumatic diseases.* 2015;74(5):921-7.
789 30. Hurley A, Smith M, Karpova T, Hasley RB, Belkina N, Shaw S, et al. Enhanced effector
790 function of CD8(+) T cells from healthy controls and HIV-infected patients occurs

through thrombin activation of protease-activated receptor 1. *The Journal of infectious diseases.* 2013;207(4):638-50.

31. Green SA, Smith M, Hasley RB, Stephany D, Harned A, Nagashima K, et al. Activated platelet-T-cell conjugates in peripheral blood of patients with HIV infection: coupling coagulation/inflammation and T cells. *AIDS (London, England).* 2015;29(11):1297-308.
32. Mudd JC, Panigrahi S, Kyi B, Moon SH, Manion MM, Younes SA, et al. Inflammatory Function of CX3CR1+ CD8+ T Cells in Treated HIV Infection Is Modulated by Platelet Interactions. *The Journal of infectious diseases.* 2016;214(12):1808-16.
33. Chen H, Smith M, Herz J, Li T, Hasley R, Le Saout C, et al. The role of protease-activated receptor 1 signaling in CD8 T cell effector functions. *iScience.* 2021;24(11):103387.
34. Coughlin SR. How the protease thrombin talks to cells. *Proceedings of the National Academy of Sciences of the United States of America.* 1999;96(20):11023-7.
35. Coughlin SR. Thrombin signalling and protease-activated receptors. *Nature.* 2000;407(6801):258-64.
36. Soh UJ, Dores MR, Chen B, and Trejo J. Signal transduction by protease-activated receptors. *British journal of pharmacology.* 2010;160(2):191-203.
37. Sambrano GR, Weiss EJ, Zheng YW, Huang W, and Coughlin SR. Role of thrombin signalling in platelets in haemostasis and thrombosis. *Nature.* 2001;413(6851):74-8.
38. Kahn ML, Zheng YW, Huang W, Bigornia V, Zeng D, Moff S, et al. A dual thrombin receptor system for platelet activation. *Nature.* 1998;394(6694):690-4.
39. Ishihara H, Zeng D, Connolly AJ, Tam C, and Coughlin SR. Antibodies to protease-activated receptor 3 inhibit activation of mouse platelets by thrombin. *Blood.* 1998;91(11):4152-7.
40. Xu WF, Andersen H, Whitmore TE, Presnell SR, Yee DP, Ching A, et al. Cloning and characterization of human protease-activated receptor 4. *Proceedings of the National Academy of Sciences of the United States of America.* 1998;95(12):6642-6.
41. Hollenberg MD. PARs in the stars: proteinase-activated receptors and astrocyte function. Focus on "Thrombin (PAR-1)-induced proliferation in astrocytes via MAPK involves multiple signaling pathways". *American journal of physiology Cell physiology.* 2002;283(5):C1347-50.
42. Ramachandran R, Noorbakhsh F, Defea K, and Hollenberg MD. Targeting proteinase-activated receptors: therapeutic potential and challenges. *Nature reviews Drug discovery.* 2012;11(1):69-86.
43. Wang T, Lee MH, Choi E, Pardo-Villamizar CA, Lee SB, Yang IH, et al. Granzyme B-induced neurotoxicity is mediated via activation of PAR-1 receptor and Kv1.3 channel. *PLoS One.* 2012;7(8):e43950.
44. Zhao P, Metcalf M, and Bunnett NW. Biased signaling of protease-activated receptors. *Frontiers in endocrinology.* 2014;5:67.
45. Lee PR, Johnson TP, Gnanapavan S, Giovannoni G, Wang T, Steiner JP, et al. Protease-activated receptor-1 activation by granzyme B causes neurotoxicity that is augmented by interleukin-1beta. *J Neuroinflammation.* 2017;14(1):131.
46. Cooper DM, Pechkovsky DV, Hackett TL, Knight DA, and Granville DJ. Granzyme K activates protease-activated receptor-1. *PLoS One.* 2011;6(6):e21484.

835 47. Sharma M, Merkulova Y, Raithatha S, Parkinson LG, Shen Y, Cooper D, et al.
836 Extracellular granzyme K mediates endothelial activation through the cleavage of
837 protease-activated receptor-1. *The FEBS journal.* 2016;283(9):1734-47.
838 48. Bovenschen N, Quadir R, van den Berg AL, Brenkman AB, Vandenberghe I, Devreese
839 B, et al. Granzyme K displays highly restricted substrate specificity that only partially
840 overlaps with granzyme A. *J Biol Chem.* 2009;284(6):3504-12.
841 49. Suidan HS, Bouvier J, Schaerer E, Stone SR, Monard D, and Tschopp J. Granzyme A
842 released upon stimulation of cytotoxic T lymphocytes activates the thrombin receptor on
843 neuronal cells and astrocytes. *Proc Natl Acad Sci U S A.* 1994;91(17):8112-6.
844 50. Kaiserman D, Zhao P, Rowe CL, Leong A, Barlow N, Joeckel LT, et al. Granzyme K
845 initiates IL-6 and IL-8 release from epithelial cells by activating protease-activated
846 receptor 2. *PLoS One.* 2022;17(7):e0270584.
847 51. Zeglinski MR, and Granville DJ. Granzymes in cardiovascular injury and disease.
848 *Cellular signalling.* 2020;76:109804.
849 52. Arias M, Martinez-Lostao L, Santiago L, Ferrandez A, Granville DJ, and Pardo J. The
850 Untold Story of Granzymes in Oncoimmunology: Novel Opportunities with Old
851 Acquaintances. *Trends Cancer.* 2017;3(6):407-22.
852 53. Jonsson AH, Zhang F, Dunlap G, Gomez-Rivas E, Watts GFM, Faust HJ, et al.
853 Granzyme K(+) CD8 T cells form a core population in inflamed human tissue. *Sci Transl*
854 *Med.* 2022;14(649):eabo0686.
855 54. Mahrus S, and Craik CS. Selective chemical functional probes of granzymes A and B
856 reveal granzyme B is a major effector of natural killer cell-mediated lysis of target cells.
857 *Chem Biol.* 2005;12(5):567-77.
858 55. Plasman K, Demol H, Bird PI, Gevaert K, and Van Damme P. Substrate specificities of
859 the granzyme tryptases A and K. *J Proteome Res.* 2014;13(12):6067-77.
860 56. !!! INVALID CITATION !!! (52).
861 57. Harker JA, Wong KA, Dallari S, Bao P, Dolgoter A, Jo Y, et al. Interleukin-27R
862 Signaling Mediates Early Viral Containment and Impacts Innate and Adaptive Immunity
863 after Chronic Lymphocytic Choriomeningitis Virus Infection. *Journal of virology.*
864 2018;92(12).
865 58. Haghverdi L, Lun ATL, Morgan MD, and Marioni JC. Batch effects in single-cell RNA-
866 sequencing data are corrected by matching mutual nearest neighbors. *Nat Biotechnol.*
867 2018;36(5):421-7.
868 59. Anderson KG, Sung H, Skon CN, Lefrancois L, Deisinger A, Vezys V, et al. Cutting
869 edge: intravascular staining redefines lung CD8 T cell responses. *J Immunol.*
870 2012;189(6):2702-6.
871 60. Masopust D, Vezys V, Marzo AL, and Lefrancois L. Preferential localization of effector
872 memory cells in nonlymphoid tissue. *Science (New York, NY.* 2001;291(5512):2413-7.
873 61. Purton JF, Martin CE, and Surh CD. Enhancing T cell memory: IL-7 as an adjuvant to
874 boost memory T-cell generation. *Immunol Cell Biol.* 2008;86(5):385-6.
875 62. Kang SS, and McGavern DB. Lymphocytic choriomeningitis infection of the central
876 nervous system. *Frontiers in bioscience : a journal and virtual library.* 2008;13:4529-43.
877 63. Baccala R, Welch MJ, Gonzalez-Quintial R, Walsh KB, Teijaro JR, Nguyen A, et al.
878 Type I interferon is a therapeutic target for virus-induced lethal vascular damage.
879 *Proceedings of the National Academy of Sciences of the United States of America.*
880 2014;111(24):8925-30.

881 64. Wherry EJ, Teichgraber V, Becker TC, Masopust D, Kaech SM, Antia R, et al. Lineage
882 relationship and protective immunity of memory CD8 T cell subsets. *Nature*
883 *immunology.* 2003;4(3):225-34.
884 65. Wherry EJ, Blattman JN, Murali-Krishna K, van der Most R, and Ahmed R. Viral
885 persistence alters CD8 T-cell immunodominance and tissue distribution and results in
886 distinct stages of functional impairment. *Journal of virology.* 2003;77(8):4911-27.
887 66. Joshi NS, Cui W, Chandele A, Lee HK, Urso DR, Hagman J, et al. Inflammation directs
888 memory precursor and short-lived effector CD8(+) T cell fates via the graded expression
889 of T-bet transcription factor. *Immunity.* 2007;27(2):281-95.
890 67. Sarkar S, Kalia V, Haining WN, Konieczny BT, Subramaniam S, and Ahmed R.
891 Functional and genomic profiling of effector CD8 T cell subsets with distinct memory
892 fates. *The Journal of experimental medicine.* 2008;205(3):625-40.
893 68. Chang JT, Wherry EJ, and Goldrath AW. Molecular regulation of effector and memory T
894 cell differentiation. *Nature immunology.* 2014;15(12):1104-15.
895 69. Herndler-Brandstetter D, Ishigame H, Shinnakasu R, Plajer V, Stecher C, Zhao J, et al.
896 KLRG1(+) Effector CD8(+) T Cells Lose KLRG1, Differentiate into All Memory T Cell
897 Lineages, and Convey Enhanced Protective Immunity. *Immunity.* 2018;48(4):716-29 e8.
898 70. Perez-Gutierrez L, and Ferrara N. Biology and therapeutic targeting of vascular
899 endothelial growth factor A. *Nat Rev Mol Cell Biol.* 2023;24(11):816-34.
900 71. Mor F, Quintana FJ, and Cohen IR. Angiogenesis-inflammation cross-talk: vascular
901 endothelial growth factor is secreted by activated T cells and induces Th1 polarization. *J*
902 *Immunol.* 2004;172(7):4618-23.
903 72. Wang QR, Wang F, Zhu WB, Lei J, Huang YH, Wang BH, et al. GM-CSF accelerates
904 proliferation of endothelial progenitor cells from murine bone marrow mononuclear cells
905 in vitro. *Cytokine.* 2009;45(3):174-8.
906 73. Bussolino F, Wang JM, Defilippi P, Turrini F, Sanavio F, Edgell CJ, et al. Granulocyte-
907 and granulocyte-macrophage-colony stimulating factors induce human endothelial cells
908 to migrate and proliferate. *Nature.* 1989;337(6206):471-3.
909 74. Biedermann BC. Vascular endothelium: checkpoint for inflammation and immunity.
910 *News in physiological sciences : an international journal of physiology produced jointly*
911 *by the International Union of Physiological Sciences and the American Physiological*
912 *Society.* 2001;16:84-8.
913 75. Danese S, Dejana E, and Fiocchi C. Immune regulation by microvascular endothelial
914 cells: directing innate and adaptive immunity, coagulation, and inflammation. *J Immunol.*
915 2007;178(10):6017-22.
916 76. Amersfoort J, Eelen G, and Carmeliet P. Immunomodulation by endothelial cells -
917 partnering up with the immune system? *Nature reviews.* 2022;22(9):576-88.
918 77. Zhang L, Gao S, White Z, Dai Y, Malik AB, and Rehman J. Single-cell transcriptomic
919 profiling of lung endothelial cells identifies dynamic inflammatory and regenerative
920 subpopulations. *JCI Insight.* 2022;7(11).
921 78. Godoy RS, Cober ND, Cook DP, McCourt E, Deng Y, Wang L, et al. Single-cell
922 transcriptomic atlas of lung microvascular regeneration after targeted endothelial cell
923 ablation. *Elife.* 2023;12.
924 79. Niethamer TK, Stabler CT, Leach JP, Zepp JA, Morley MP, Babu A, et al. Defining the
925 role of pulmonary endothelial cell heterogeneity in the response to acute lung injury.
926 *Elife.* 2020;9.

927 80. Rodor J, Chen SH, Scanlon JP, Monteiro JP, Caudrillier A, Sweta S, et al. Single-cell
928 RNA sequencing profiling of mouse endothelial cells in response to pulmonary arterial
929 hypertension. *Cardiovasc Res.* 2022;118(11):2519-34.
930 81. Jerkic M, Rivas-Elena JV, Prieto M, Carron R, Sanz-Rodriguez F, Perez-Barriocanal F, et
931 al. Endoglin regulates nitric oxide-dependent vasodilatation. *FASEB journal : official*
932 *publication of the Federation of American Societies for Experimental Biology.*
933 2004;18(3):609-11.
934 82. Toporsian M, Gros R, Kabir MG, Vera S, Govindaraju K, Eidelman DH, et al. A role for
935 endoglin in coupling eNOS activity and regulating vascular tone revealed in hereditary
936 hemorrhagic telangiectasia. *Circulation research.* 2005;96(6):684-92.
937 83. Kretschmer S, Dethlefsen I, Hagner-Benes S, Marsh LM, Garn H, and Konig P.
938 Visualization of intrapulmonary lymph vessels in healthy and inflamed murine lung using
939 CD90/Thy-1 as a marker. *PLoS One.* 2013;8(2):e55201.
940 84. Levine JH, Simonds EF, Bendall SC, Davis KL, Amir el AD, Tadmor MD, et al. Data-
941 Driven Phenotypic Dissection of AML Reveals Progenitor-like Cells that Correlate with
942 Prognosis. *Cell.* 2015;162(1):184-97.
943 85. Li Q, Wei S, Li Y, Wu F, Qin X, Li Z, et al. Blocking of programmed cell death-ligand 1
944 (PD-L1) expressed on endothelial cells promoted the recruitment of CD8(+)IFN-
945 gamma(+) T cells in atherosclerosis. *Inflammation research : official journal of the*
946 *European Histamine Research Society [et al].* 2023;72(4):783-96.
947 86. Yu QC, Song W, Wang D, and Zeng YA. Identification of blood vascular endothelial
948 stem cells by the expression of protein C receptor. *Cell Res.* 2016;26(10):1079-98.
949 87. Thiyagarajan M, Cheng T, and Zlokovic BV. Endothelial cell protein C receptor: role
950 beyond endothelium? *Circulation research.* 2007;100(2):155-7.
951 88. Zhu Z, Li T, Chen J, Kumar J, Kumar P, Qin J, et al. The Role of Inflammation and
952 Immune Activation on Circulating Endothelial Progenitor Cells in Chronic HIV
953 Infection. *Frontiers in immunology.* 2021;12:663412.
954 89. Kushner EJ, MacEneaney OJ, Morgan RG, Van Engelenburg AM, Van Guilder GP, and
955 DeSouza CA. CD31+ T cells represent a functionally distinct vascular T cell phenotype.
956 *Blood Cells Mol Dis.* 2010;44(2):74-8.
957 90. Pilling JE, Galvin A, Robins AM, Sewell HF, and Mahida YR. Expression of alpha5
958 (CD49e) and alpha6 (CD49f) integrin subunits on T cells in the circulation and the
959 lamina propria of normal and inflammatory bowel disease colonic mucosa. *Scandinavian*
960 *journal of immunology.* 1998;48(4):425-8.
961 91. Singh V, Kaur R, Kumari P, Pasricha C, and Singh R. ICAM-1 and VCAM-1:
962 Gatekeepers in various inflammatory and cardiovascular disorders. *Clin Chim Acta.*
963 2023;548:117487.
964 92. Groten SA, Smit ER, Janssen EFJ, van den Eshof BL, van Alphen FPJ, van der Zwaan C,
965 et al. Multi-omics delineation of cytokine-induced endothelial inflammatory states.
966 *Commun Biol.* 2023;6(1):525.
967 93. Nakamichi M, Akishima-Fukasawa Y, Fujisawa C, Mikami T, Onishi K, and Akasaka Y.
968 Basic Fibroblast Growth Factor Induces Angiogenic Properties of Fibrocytes to Stimulate
969 Vascular Formation during Wound Healing. *The American journal of pathology.*
970 2016;186(12):3203-16.
971 94. Arnaoutova I, and Kleinman HK. In vitro angiogenesis: endothelial cell tube formation
972 on gelled basement membrane extract. *Nature protocols.* 2010;5(4):628-35.

95. Zhang C, Srinivasan Y, Arlow DH, Fung JJ, Palmer D, Zheng Y, et al. High-resolution crystal structure of human protease-activated receptor 1. *Nature.* 2012;492(7429):387-92.
96. Brass LF, Pizarro S, Ahuja M, Belmonte E, Blanchard N, Stadel JM, et al. Changes in the structure and function of the human thrombin receptor during receptor activation, internalization, and recycling. *J Biol Chem.* 1994;269(4):2943-52.
97. O'Brien PJ, Prevost N, Molino M, Hollinger MK, Woolkalis MJ, Woulfe DS, et al. Thrombin responses in human endothelial cells. Contributions from receptors other than PAR1 include the transactivation of PAR2 by thrombin-cleaved PAR1. *J Biol Chem.* 2000;275(18):13502-9.
98. Qiu C, Xie Q, Zhang D, Chen Q, Hu J, and Xu L. GM-CSF induces cyclin D1 expression and proliferation of endothelial progenitor cells via PI3K and MAPK signaling. *Cell Physiol Biochem.* 2014;33(3):784-95.
99. Newman PJ. Switched at birth: a new family for PECAM-1. *The Journal of clinical investigation.* 1999;103(1):5-9.
100. Fornasa G, Groyer E, Clement M, Dimitrov J, Compain C, Gaston AT, et al. TCR stimulation drives cleavage and shedding of the ITIM receptor CD31. *J Immunol.* 2010;184(10):5485-92.
101. Ma L, Mauro C, Cornish GH, Chai JG, Coe D, Fu H, et al. Ig gene-like molecule CD31 plays a nonredundant role in the regulation of T-cell immunity and tolerance. *Proceedings of the National Academy of Sciences of the United States of America.* 2010;107(45):19461-6.
102. Delacher M, Schmidleithner L, Simon M, Stuve P, Sanderink L, Hotz-Wagenblatt A, et al. The effector program of human CD8 T cells supports tissue remodeling. *The Journal of experimental medicine.* 2024;221(2).
103. Deliyanti D, Figgett WA, Gebhardt T, Trapani JA, Mackay F, and Wilkinson-Berka JL. CD8(+) T Cells Promote Pathological Angiogenesis in Ocular Neovascular Disease. *Arterioscler Thromb Vasc Biol.* 2023;43(4):522-36.
104. Pober JS, and Sessa WC. Evolving functions of endothelial cells in inflammation. *Nature reviews.* 2007;7(10):803-15.
105. Frebel H, Nindl V, Schuepbach RA, Braunschweiler T, Richter K, Vogel J, et al. Programmed death 1 protects from fatal circulatory failure during systemic virus infection of mice. *The Journal of experimental medicine.* 2012;209(13):2485-99.
106. Lee C, Kim MJ, Kumar A, Lee HW, Yang Y, and Kim Y. Vascular endothelial growth factor signaling in health and disease: from molecular mechanisms to therapeutic perspectives. *Signal Transduct Target Ther.* 2025;10(1):170.
107. Li C, Issa R, Kumar P, Hampson IN, Lopez-Novoa JM, Bernabeu C, et al. CD105 prevents apoptosis in hypoxic endothelial cells. *Journal of cell science.* 2003;116(Pt 13):2677-85.
108. Lin Y, Banno K, Gil CH, Myslinski J, Hato T, Shelley WC, et al. Origin, prospective identification, and function of circulating endothelial colony-forming cells in mice and humans. *JCI Insight.* 2023;8(5).
109. Weil BR, Kushner EJ, Diehl KJ, Greiner JJ, Stauffer BL, and Desouza CA. CD31+ T cells, endothelial function and cardiovascular risk. *Heart Lung Circ.* 2011;20(10):659-62.
110. Lopez P, Rodriguez-Carrio J, Martinez-Zapico A, Caminal-Montero L, and Suarez A. Senescent profile of angiogenic T cells from systemic lupus erythematosus patients. *J Leukoc Biol.* 2016;99(3):405-12.

111. de Boer SA, Reijrink M, Abdulahad WH, Hoekstra ES, Slart R, Heerspink HJL, et al. Angiogenic T cells are decreased in people with type 2 diabetes mellitus and recruited by the dipeptidyl peptidase-4 inhibitor Linagliptin: A subanalysis from a randomized, placebo-controlled trial (RELEASE study). *Diabetes Obes Metab.* 2020;22(7):1220-5.
112. Kul A, Ozturk N, Kurt AK, and Arslan Y. Detection of Angiogenic T Cells and Endothelial Progenitor Cells in Behcet Disease and Determination of Their Relationship with Disease Activity. *Life (Basel).* 2023;13(6).
113. Manetti M, Pratesi S, Romano E, Bellando-Randone S, Rosa I, Guiducci S, et al. Angiogenic T cell expansion correlates with severity of peripheral vascular damage in systemic sclerosis. *PLoS One.* 2017;12(8):e0183102.
114. Zhang G, Liu Y, Qiu Y, Zhang J, Sun J, Zhou Z, et al. Circulating senescent angiogenic T cells are linked with endothelial dysfunction and systemic inflammation in hypertension. *J Hypertens.* 2021;39(5):970-8.
115. Panigrahi S, Chen B, Fang M, Potashnikova D, Komissarov AA, Lebedeva A, et al. CX3CL1 and IL-15 Promote CD8 T cell chemoattraction in HIV and in atherosclerosis. *PLoS Pathog.* 2020;16(9):e1008885.
116. Chamberlain CM, and Granville DJ. The role of Granzyme B in atheromatous diseases. *Canadian journal of physiology and pharmacology.* 2007;85(1):89-95.
117. Choy JC, McDonald PC, Suarez AC, Hung VH, Wilson JE, McManus BM, et al. Granzyme B in atherosclerosis and transplant vascular disease: association with cell death and atherosclerotic disease severity. *Modern pathology : an official journal of the United States and Canadian Academy of Pathology, Inc.* 2003;16(5):460-70.
118. Richardson KC, Jung K, Pardo J, Turner CT, and Granville DJ. Noncytotoxic Roles of Granzymes in Health and Disease. *Physiology (Bethesda).* 2022;37(6):323-48.
119. Ikemoto T, Hojo Y, Kondo H, Takahashi N, Hirose M, Nishimura Y, et al. Plasma granzyme B as a predicting factor of coronary artery disease--clinical significance in patients with chronic renal failure. *Journal of cardiology.* 2009;54(3):409-15.
120. Hendel A, Hiebert PR, Boivin WA, Williams SJ, and Granville DJ. Granzymes in age-related cardiovascular and pulmonary diseases. *Cell death and differentiation.* 2010;17(4):596-606.
121. Xu T, Zhu HX, You X, Ma JF, Li X, Luo PY, et al. Single-cell profiling reveals pathogenic role and differentiation trajectory of granzyme K+CD8+ T cells in primary Sjogren's syndrome. *JCI Insight.* 2023;8(8).
122. Hiebert PR, Boivin WA, Abraham T, Pazooki S, Zhao H, and Granville DJ. Granzyme B contributes to extracellular matrix remodeling and skin aging in apolipoprotein E knockout mice. *Experimental gerontology.* 2011;46(6):489-99.

1057 **Figure Legends**

1058 **Figure 1. PAR1 expression is modulated in LCMVGp33-specific CD8 T lymphocytes during**
1059 **acute LCMV infection.**

1060 *In vivo* expression of PAR1 in splenic cells from naïve C57BL/6-F2r$^{fl/fl}$ (n= 5) and C57BL/6 (n=
1061 5) mice analyzed by flow cytometry. **(A)** Cells were analyzed after gating on live cells, and singlets
1062 and CD45^{+} lymphocytes. Representative contour plots gating cell types: NK cells (CD3^{-}NK1.1^{+}),
1063 B cells (MHCII^{+}B220^{+}), CD4 (CD3^{+}CD4^{+}) and CD8 T cells (CD3^{+}CD8^{+}). **(B)** Representative
1064 histogram of tdTomato (PAR1) expression in CD4 and CD8 T cells, B cells and NK cells from
1065 C57BL/6 mice (solid grey) and C57BL/6-F2r$^{fl/fl}$ mice (black line). **(C)** Median Fluorescence
1066 Intensity (MFI) of tdTomato expression of total splenic cells from C57BL/6 mice (SP) and B cells,
1067 NK and CD4 and CD8 T cells and NK cells from C57BL/6-F2r$^{fl/fl}$ mice. **(D)** Relative *F2r* mRNA
1068 expression in sorted B cells and purified by magnetic isolation of CD4 and CD8 T cells from
1069 C57BL/6-F2r$^{fl/fl}$ mice (n= 6). **(E)** C57BL/6-F2r$^{fl/fl}$ mice were infected with LCMVArm strain (2 x
1070 10^{5} pfu, i.v). Splenic and lung cells were assessed at day 6 and 21 p.i. by flow cytometry. **(F)**
1071 Representative histogram of tdTomato (tdT) expression in total CD8 T cells from naïve (N) and
1072 infected mice at day 6 and 21 p.i. (solid gray). Overlayed, tdTomato expression in LCMVGp33-
1073 specific CD8 T cells detected by H2-D^{b}LCMVGp33 pentamer staining (red line). **(F)** Median
1074 Fluorescence Intensity (MFI) of tdTomato expression in LCMVGp33-specific CD8 T cells
1075 detected by H2-D^{b}LCMVGp33 pentamer staining. Dashed line represents level expression of total
1076 naïve CD8 T cells. **(G)** Representative plot of lung endothelial cells (EC). After excluding dead
1077 cells and doublets, ECs were gated as CD326^{-}CD45^{-}CD31^{+}. Frequency and cell count of lung
1078 endothelial cells from naïve (N) and infected mice at days 6 and 21 p.i. Frequencies of ECs are

1079 expressed as frequency of total live cells. **(H)** Median Fluorescence Intensity (MFI) of tdTomato
1080 expression in lung ECs from naïve (N) and infected mice (day 6 and day 21p.i.).
1081 The bar graph is represented by box and whisker showing the median value with first and third
1082 quartiles in the box, with whiskers extending to the minimum and maximum values. The data in
1083 line graphs represent mean±SEM in each time point. Data are pooled from three independent
1084 experiments with 5-9 naïve animals (C, E and F) and 8-17 per time point (F and H). Statistical
1085 analysis was performed using non-parametric Mann-Whitney test. P value < 0.05 was considered
1086 significant.
1087
1088 **Figure 2. Angiogenic CD8 T cells promote endothelial recovery during acute viral infection.**
1089 **(A)** Schematic presentation of CD8 T cell depletion. C57BL/6-F2r$^{fl/fl}$ mice were infected with
1090 LCMVArm strain (2 x 10^5 pfu, i.v). At day 15 p.i mice were administered anti-CD8α mAb and
1091 IgG2b isotype for control mice. Frequency and cell count of CD8 T cells at day 21p.i in CD8 T
1092 cell depleted mice and IgG treated control mice assessed by flow cytometry. **(B)** Lung endothelial
1093 cell frequency and count from CD8 T cell depleted and control mice at day 21 p.i. Frequencies of
1094 ECs are expressed as frequency of total live cells. **(C)** Representative contour plot of CD31^{high} and
1095 CD309 expression by lung CD8 T cells from naïve mice and infected mice. Frequency and cell
1096 count of CD31^{high}CD8 T cells from naïve (N) mice and infected mice at day 6 and 21 p.i. **(D)** Lung
1097 CD31^{high} and CD31^{neg} CD8 T cells, representative contour plot of secretion of IFNγ, TNFα
1098 secretion and CD107a upon *in vitro* stimulation with LCMVGp33-44 peptide. DMSO was used as
1099 control. **(E)** Representative contour plot of KLRG1 and CD127 expression by LCMVGp33-
1100 specific CD8 T cells. Frequency of KLRG1$^-$CD127$^+$ (R1), KLRG1$^+$CD127$^+$ (R2) and
1101 KLRG1$^+$CD127$^-$ and KLRG1$^-$CD127$^-$ (R3+R4) LCMVGp33 specific CD8 T cells from lung at

1102 days 6 and 21 p.i.. **(F)** Lung CD31^{high} and CD31^{neg} bulk CD8 T cells were sorted from naïve mice
1103 and infected mice at 21 p.i. and stimulated *in vitro* with anti-CD3 and anti-CD28 mAbs coated
1104 plate for 3 days. Detection of VEGF in the supernatants of the culture. The bar graphs are
1105 represented by box and whisker showing the median value with first and third quartiles in the box,
1106 with whiskers extending to the minimum and maximum values. The data in line graphs represent
1107 mean±SEM in each time point. Data are pooled from two independent experiments with 8 naïve
1108 animals (A and B) and 7-16 per time point (C, D and E). Sorted cells from 3 naïve and 6 infected
1109 mice per time point (G). Statistical analysis was performed using non-parametric Mann-Whitney
1110 test. P value < 0.05 was considered significant.
1111
1112 **Figure 3. CD31^{high}CD8 T cells are associated with endothelial that express a regenerative**
1113 **phenotype.**
1114 **(A)** Unsupervised clustering analysis of lung endothelial cells using phonograph (k= 100). The
1115 heatmap represent mean fluorescence intensity of CD31, PDL1, tdTomato, CD34, CD309,
1116 VCAM-1, CD105, CD90.2 and CD201 expression in ECs. Bubble plots represent the mean
1117 frequency of each cluster from naïve and infected mice at day 6 and 21 p.i. **(B)** Relationship
1118 between frequency of Cluster 6 and lung CD31^{high}CD8 T cells. Data are pooled from two
1119 independent experiments with 7 naïve (A and B) and 8-10 per time point animals (A and B).
1120 Correlation were performed using non-parametric Spearman correlation and p value $\leqslant$ 0.01 was
1121 considered significant.
1122
1123 **Figure 4. Proinflammatory phenotype of CD8 T_{ang} correlates to ASCVD risk in PWH.**
1124 Circulating T_{ang} were analyzed in PBMCs from PWH (n= 25, red symbols) and PWoH (n= 17,
1125 blue symbols) by flowcytometry. After gating on live cells and singlets, CD4 and CD8 T cells

1126 were analyzed based on expression of CD31 and CXCR4: **(A)** Representative contour plots for
1127 gating angiogenic T cells, CD4 T_{ang} ($CD31^+CXCR4^+$) and CD8 T_{ang} ($CD31^+CXCR4^+$). **(B)**
1128 Frequency of CD4 T_{ang} and CD8 T_{ang} from PWH and PWoH. CD4 T_{ang} and CD8 T_{ang} expression
1129 of: (**C**) CX3CR1 and PAR1 **(D)** CD49f and PAR1 **(E)** granzyme A (GZMA) and B (GZMB). **F,**
1130 **G and H.** Relationship between expression of CD4 and CD8 T_{ang} cells and atherosclerotic
1131 cardiovascular disease (ASCVD) risk score in PWH. **(I)** Relationship between expression of
1132 plasma levels of sVCAM-1, sICAM-1, IL-6 and granzyme A in PWH (n= 25). The bar graph is
1133 represented by box and whisker showing the median value with first and third quartiles in the box,
1134 with whiskers extending to the minimum and maximum values. Statistical analysis was performed
1135 using non-parametric Mann-Whitney test. P value < 0.05 was considered significant. Correlations
1136 were performed using non-parametric Spearman correlation and p value $\leqslant$ 0.01 was considered
1137 significant.
1138
1139 **Figure 5. *In vitro*, CD8 T_{ang} cells from PWH induced shedding of sICAM-1 and sVCAM-1 by**
1140 **endothelial cells.**
1141 CD8 T_{ang} from PWH (n= 10, red symbols) and PWoH (n= 10, blue symbols) were sorted and
1142 stimulated with CD3 and CD28 mAbs coated beads for 3 days and expanded in the presence of
1143 IL-2 for an additional 14 days. Activated CD8 T_{ang} cells were co-cultured with primary human
1144 umbilical vein endothelial cells HUVEC at 2 to 1 CD8 T_{ang} to HUVEC ratio for 24 hours.
1145 Supernatants were collected and measured: **(A)** Soluble vascular cell adhesion molecule 1
1146 (sVCAM1) and intracellular adhesion molecule 1 (sICAM1). **(B)** Cytokines IL-6, Angiopoietin-2
1147 (Ang-2), fibroblast growth factor (bFGF), vascular endothelial growth factor (VEGF) and IL-
1148 8/CXCL8. **(C)** Sorted CD8 T_{ang} memory cells ($CD45RA^-CD27^+$) from PWH (n= 3, opened red

1149 symbols), PWoH (n= 2, blue symbols), and HIVGag-specific CD8 T cells from PWH (n= 2, solid
1150 red symbols) were labeled with CFSE and cultured with HUVEC at a 2 to 1 ratio in Ibidi chambers
1151 for up to 12 hours. As control, HUVEC were cultured alone (black symbol). Representative phase
1152 contrast images at 2, 4, 6, 8, 10 and 12 hours with masks of tube (black line), branching point
1153 (white point), loop (labeled with number) and CD8 T_{ang} cells (red dots). **(D)** Representative
1154 fluorescent images of T_{ang} cells and HUVEC. **(E)** Fold change of median loop area of individual
1155 donors from PWH and PWoH and HIVGag-specific CD8 T cells. **(F)** Fold change of median loop
1156 area of pooled all donors. HUVEC shows mean±SEM of pooled experiments with all donors. The
1157 bar graph is represented by box and whisker showing the median value with first and third quartiles
1158 in the box, with whiskers extending to the minimum and maximum values. Line graphs represent
1159 the average of all donors. Statistical analysis was performed using non-parametric Mann-Whitney
1160 test. P value < 0.05 was considered significant.
1161
1162 **Figure 6. Activated CD8 T_{ang} cells mediate endothelial cell activation through a granzyme-**
1163 **dependent PAR1 activation**
1164 **(A)** Diagram illustrates the molecular mechanism of cleavage dependent PAR1 activation via
1165 serine proteases. Inhibition of PAR1 activation by ATAP-2 mAb and antagonist SCH530348
1166 (vorapaxar). Peptide agonist (mimics the tethered ligand) and cleavage independent PAR1
1167 activation. The figure was generated with Biorender. **(B)** Image of Granzyme A induced
1168 intracellular calcium mobilization in HUVEC. Intracellular calcium mobilization kinetics in
1169 HUVEC stimulated with granzyme A and thrombin as control. Each line represents the kinetics
1170 overtime of individual cells (lower panel). **(C, D and E)** HUVEC were stimulated with 100 nM of
1171 rh GZMA and GZMK overnight in the presence or absence of 10 μg/mL of ATAP-2 mAb or 300

1172 nM of PAR1 antagonist SCH530348. (**F, G** and **H**) HUVEC were stimulated with 100 μM of
1173 PAR1 agonist peptide (TFLLR-NH2) and peptide control (RLLFT-NH2) as positive and negative
1174 controls respectively. IL-6, IL-8/CXCL8 and Angiopoietin-2 were measured in the supernatants
1175 of the cultures. The bar graph is represented by box and whisker showing the median value with
1176 first and third quartiles in the box, with whiskers extending to the minimum and maximum values.
1177 Statistical analysis was performed using non-parametric Mann-Whitney test. P value <0.05 was
1178 considered significant.
1179

Table 1. Study groups characteristics

Demographics	**PWH (n= 25)**	**PWOH (n= 17)**
Age, yr, median (IQR)	52 (42-57.5)	48 (34-60)
Gender n (%)		
Male	22 (88)	8 (47.1)
Female	3 (12)	9 (52.9)
Ethnicity n (%)		
White	8 (32)	11 (64.8)
African American	12 (48)	3 (17.6)
Other	5 (20)	3 (17.6)
Clinical Characteristics		
Smoker ever, n (%)	8 (32)	N/A
Diabetes, n (%)	9 (36)	N/A
ASCVD risk estimator, median (IQR)[1]	7.9 (5.0-18.6)	N/A
Clinical Laboratory, median (IQR)		
Cholesterol, mg/dL[2]	168 (147-194)	N/A
HDL, mg/dL[3]	47 (41-56.3)	N/A
LDL, mg/dL[3]	99.5 (78.5-117.5)	N/A
HIV Characteristics, median (IQR)		
Viral Load copies/mL[4]	<20 (20-20)	N/A
CD4 count, cells/μL	663 (532-861.5)	N/A
ART treatment		
NRTIs, n (%)	19 (76)	N/A
NNRTIs, n (%)	4 (16)	N/A
PIs, n (%)	4 (16)	N/A
INSTIs, n (%)	14 (56)	N/A
Serum Biomarkers, median (IQR)		
sVCAM-1, pg/mL	288.5 (188.6-366.6)	
IL-6	3.7 (1.2-4.6)	
Granzyme A	256.1 (111.1-514)	
Granzyme B	920.8 (523.4-1566)	
IFNγ	289.8 (87.0-1012)	
TNFα	2.5 (1.1-4.6)	
sFASL	9.8 (3.6-24.1)	

[1] 5 out of 25 participants didn't have ASCVD risk estimator. [2] 10 out of 25 participants didn't have total cholesterol. [3] 11 out of 25 participants didn't have HDL and LDL. [4] 4 out of 25 participants have viral load 110, 70, 60 and 50 HIV RNA copies/mL respectively.

Figure 1

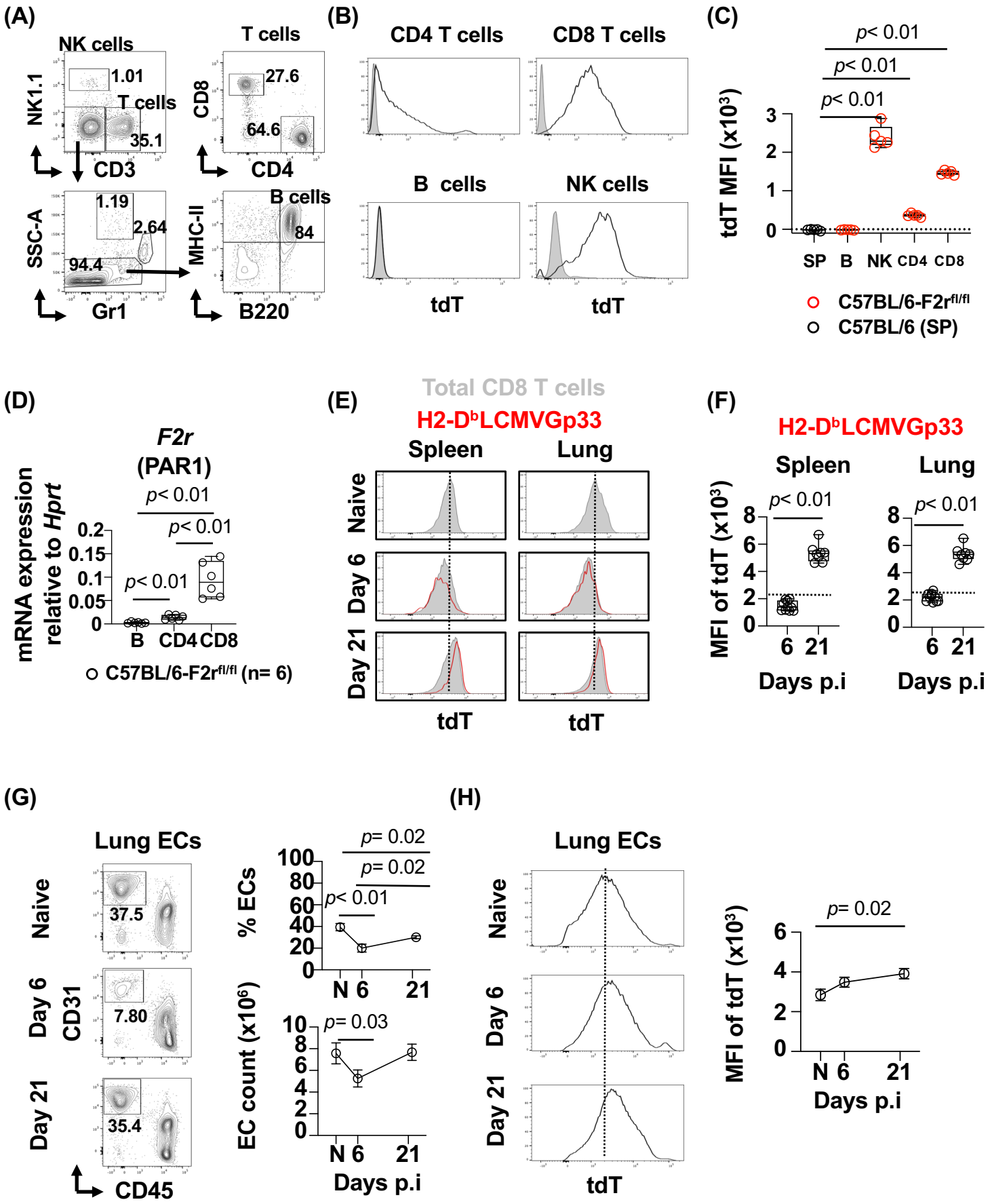
(A)
NK cells
T cells
NK1.1
CD3
1.01
35.1
CD8
CD4
27.6
64.6
SSC-A
Gr1
1.19
2.64
94.4
MHC-II
B220
B cells
84
(B)
CD4 T cells
CD8 T cells
B cells
NK cells
tdT
tdT
(C)
p< 0.01
p< 0.01
p< 0.01
tdT MFI (x10³)
SP B NK CD4 CD8
C57BL/6-F2r fl/fl
C57BL/6 (SP)
(D)
F2r
(PAR1)
mRNA expression relative to Hprt
p< 0.01
p< 0.01
p< 0.01
B CD4 CD8
C57BL/6-F2r fl/fl (n= 6)
(E)
Total CD8 T cells
H2-DbLCMVGp33
Spleen
Lung
Naive
Day 6
Day 21
tdT
tdT
(F)
H2-DbLCMVGp33
Spleen
Lung
MFI of tdT (x10³)
p< 0.01
p< 0.01
6 21
Days p.i
Days p.i
(G)
Lung ECs
Naive
Day 6
Day 21
CD31
CD45
37.5
7.80
35.4
% ECs
p= 0.02
p= 0.02
p< 0.01
N 6 21
EC count (x10⁶)
p= 0.03
N 6 21
Days p.i
(H)
Lung ECs
Naive
Day 6
Day 21
tdT
MFI of tdT (x10³)
p= 0.02
N 6 21
Days p.i

Figure 2

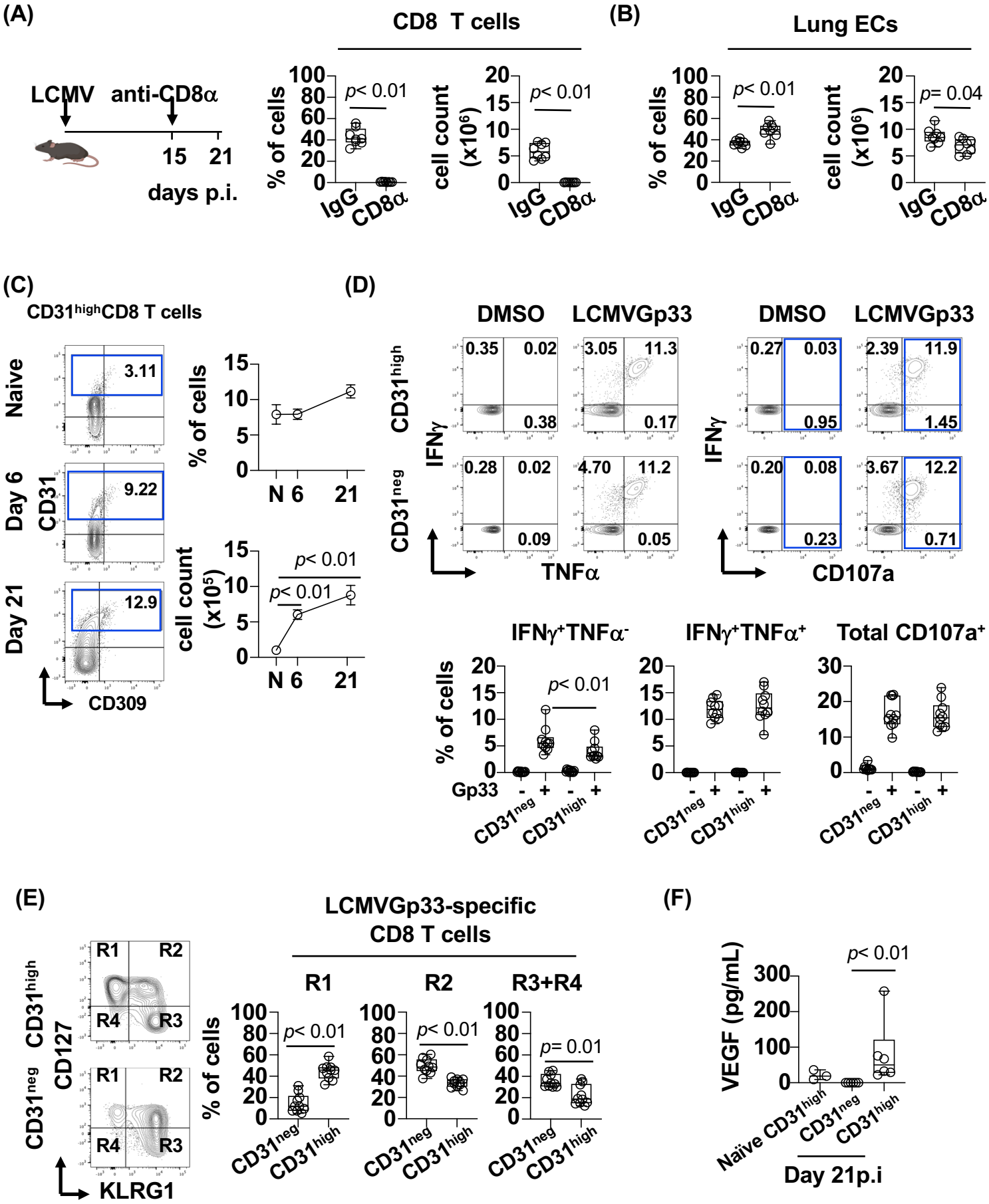
(A)
LCMV
anti-CD8α
15
21
days p.i.
CD8 T cells
% of cells
p< 0.01
IgG
CD8α
cell count (x10^6)
p< 0.01
(B)
Lung ECs
% of cells
p< 0.01
cell count (x10^6)
p= 0.04
(C)
CD31^high CD8 T cells
Naive
Day 6
Day 21
CD31
CD309
3.11
9.22
12.9
% of cells
N 6 21
cell count (x10^5)
p< 0.01
p< 0.01
(D)
DMSO
LCMVGp33
CD31^high
CD31^neg
IFNγ
TNFα
CD107a
0.35 0.02 0.38
3.05 11.3 0.17
0.28 0.02 0.09
4.70 11.2 0.05
0.27 0.03 0.95
2.39 11.9 1.45
0.20 0.08 0.23
3.67 12.2 0.71
IFNγ+TNFα-
IFNγ+TNFα+
Total CD107a+
% of cells
p< 0.01
Gp33
CD31^neg
CD31^high
(E)
LCMVGp33-specific CD8 T cells
CD31^high
CD31^neg
CD127
KLRG1
R1
R2
R3
R4
R1
R2
R3+R4
% of cells
p< 0.01
p< 0.01
p= 0.01
CD31^neg
CD31^high
(F)
VEGF (pg/mL)
p< 0.01
Naïve
CD31^high
CD31^neg
CD31^high
Day 21p.i

Figure 3

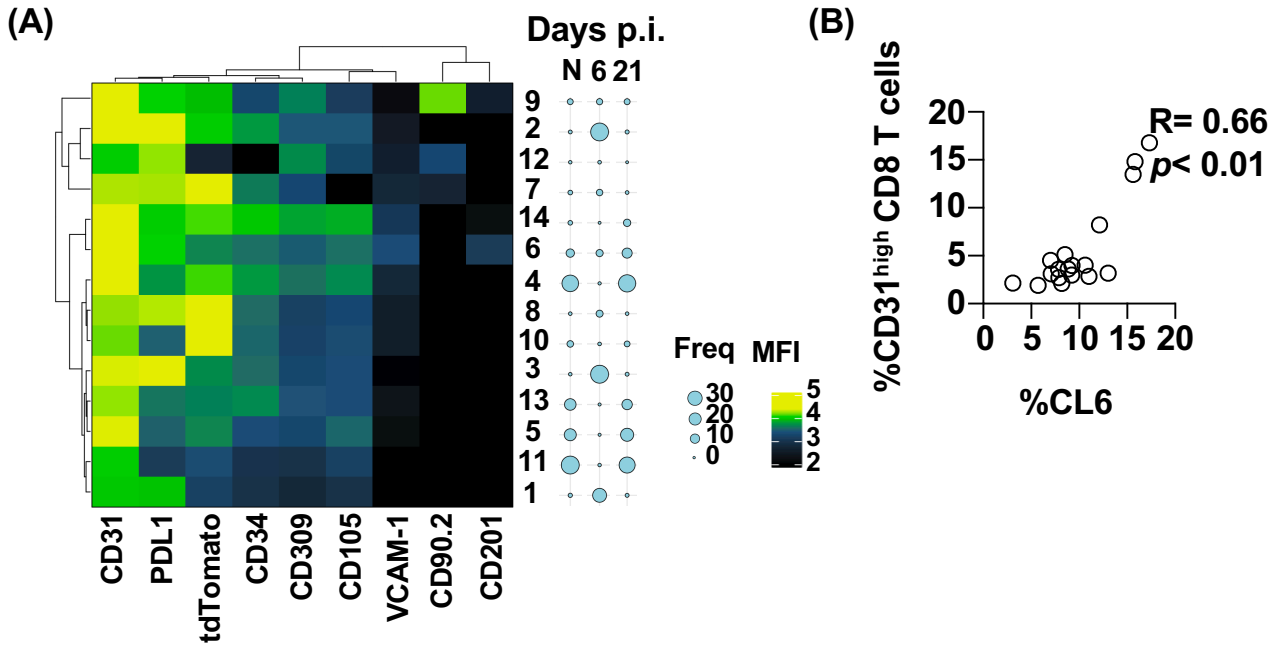
(A)
Days p.i.
N 6 21
9
2
12
7
14
6
4
8
10
3
13
5
11
1
CD31
PDL1
tdTomato
CD34
CD309
CD105
VCAM-1
CD90.2
CD201
Freq
30
20
10
0
MFI
5
4
3
2
(B)
%CD31high CD8 T cells
20
15
10
5
0
0 5 10 15 20
%CL6
R= 0.66
p< 0.01

Figure 4

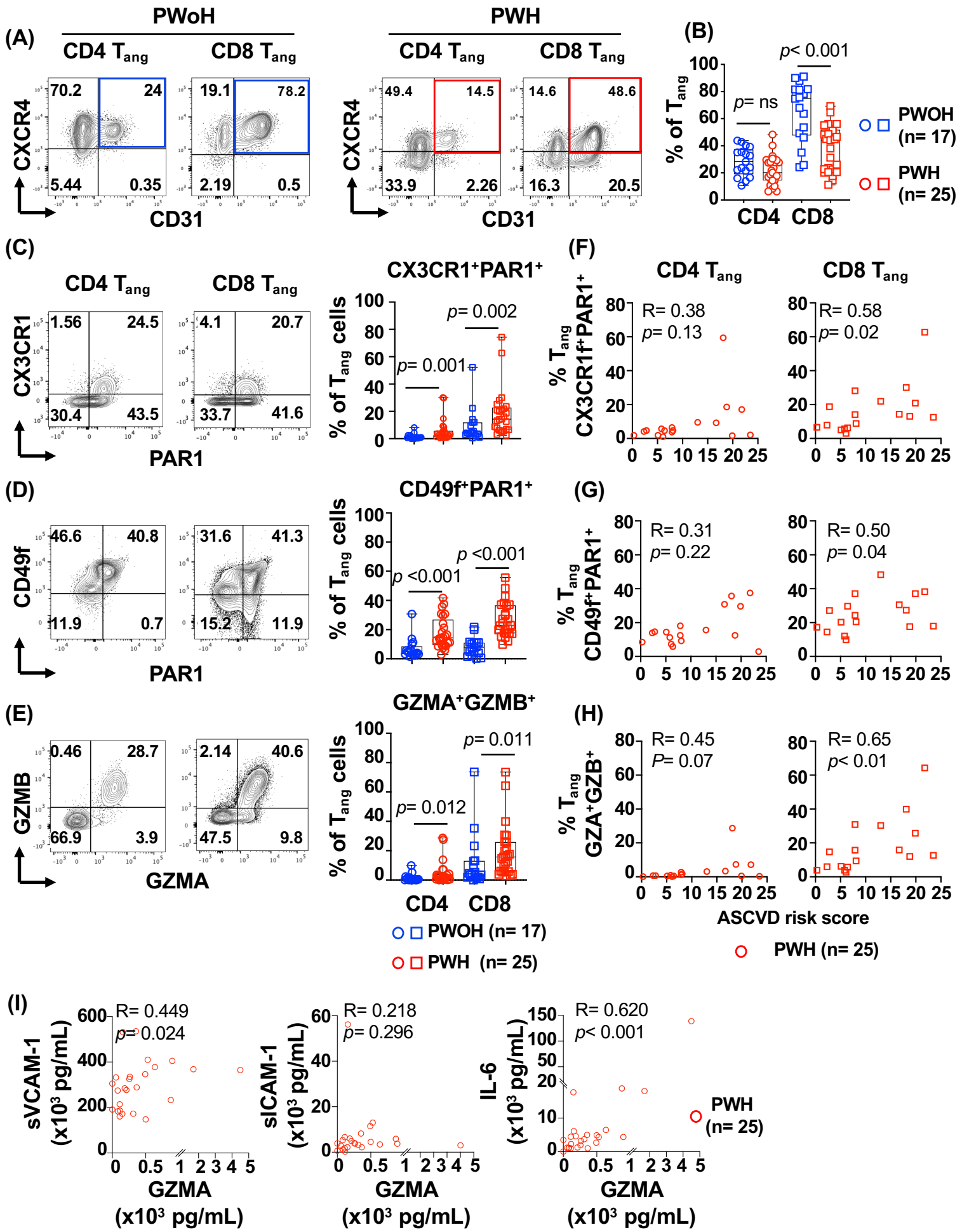
(A)
PWoH
PWH
CD4 Tang
CD8 Tang
CXCR4
CD31
70.2
24
5.44
0.35
19.1
78.2
2.19
0.5
49.4
14.5
33.9
2.26
14.6
48.6
16.3
20.5
(B)
% of Tang
p= ns
p< 0.001
CD4
CD8
PWOH (n= 17)
PWH (n= 25)
(C)
CX3CR1
PAR1
1.56
24.5
30.4
43.5
4.1
20.7
33.7
41.6
CX3CR1+PAR1+
% of Tang cells
p= 0.001
p= 0.002
(D)
CD49f
46.6
40.8
11.9
0.7
31.6
41.3
15.2
11.9
CD49f+PAR1+
p <0.001
p <0.001
(E)
GZMB
GZMA
0.46
28.7
66.9
3.9
2.14
40.6
47.5
9.8
GZMA+GZMB+
p= 0.012
p= 0.011
(F)
CX3CR1f+PAR1+
R= 0.38
p= 0.13
R= 0.58
p= 0.02
(G)
CD49f+PAR1+
R= 0.31
p= 0.22
R= 0.50
p= 0.04
(H)
GZA+GZB+
R= 0.45
P= 0.07
R= 0.65
p< 0.01
ASCVD risk score
(I)
sVCAM-1 (x10³ pg/mL)
R= 0.449
p= 0.024
sICAM-1 (x10³ pg/mL)
R= 0.218
p= 0.296
IL-6 (x10³ pg/mL)
R= 0.620
p< 0.001
GZMA (x10³ pg/mL)
PWH (n= 25)

Figure 5

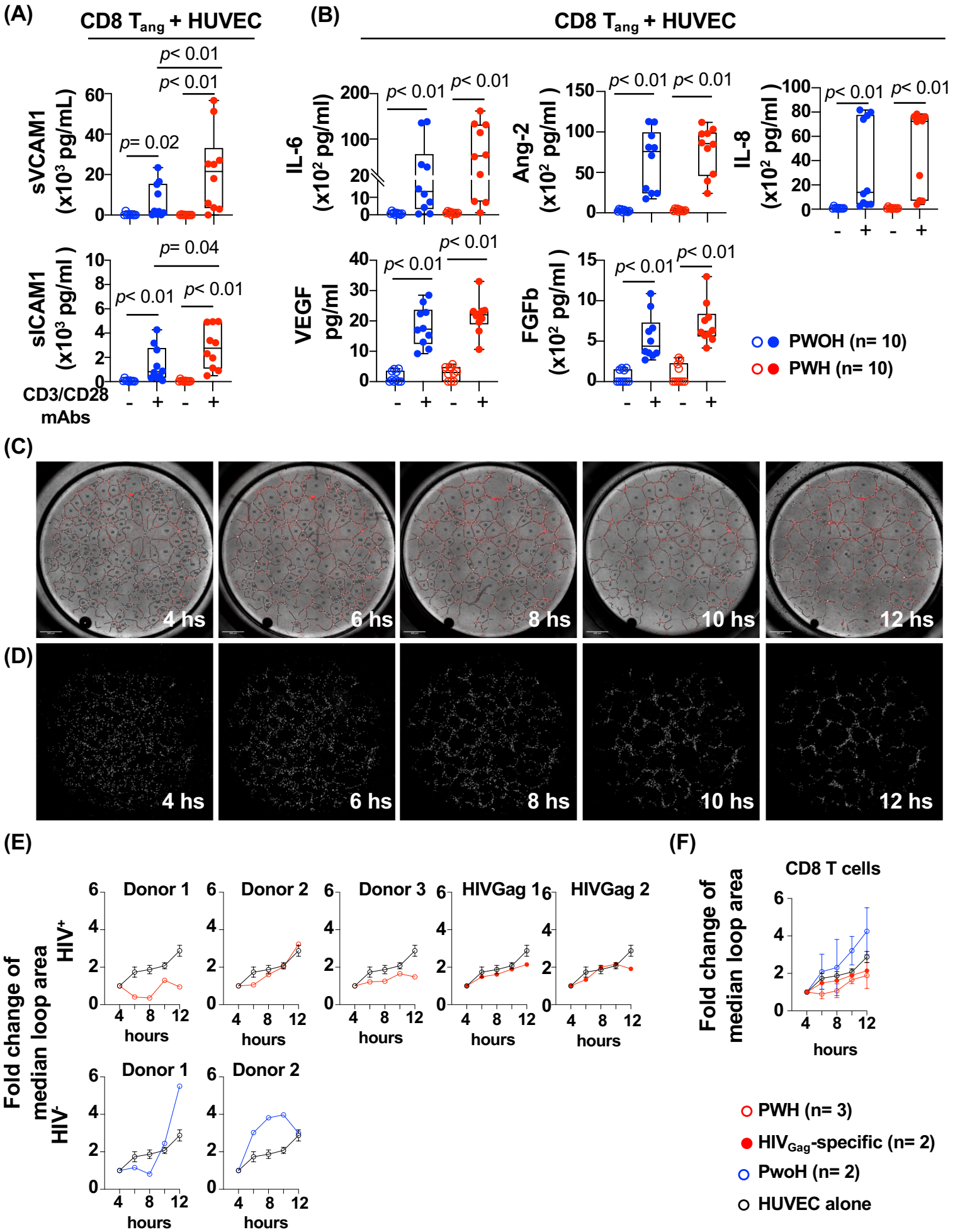
(A)
CD8 Tang + HUVEC
sVCAM1 (x10³ pg/mL)
p= 0.02
p< 0.01
p< 0.01
sICAM1 (x10³ pg/ml)
p< 0.01
p< 0.01
p= 0.04
CD3/CD28 mAbs
(B)
CD8 Tang + HUVEC
IL-6 (x10² pg/ml)
Ang-2 (x10² pg/ml)
IL-8 (x10² pg/ml)
VEGF pg/ml
FGFb (x10² pg/ml)
p< 0.01
PWOH (n= 10)
PWH (n= 10)
(C)
4 hs
6 hs
8 hs
10 hs
12 hs
(D)
4 hs
6 hs
8 hs
10 hs
12 hs
(E)
Fold change of median loop area
HIV+
HIV-
Donor 1
Donor 2
Donor 3
HIVGag 1
HIVGag 2
hours
(F)
CD8 T cells
Fold change of median loop area
hours
PWH (n= 3)
HIVGag-specific (n= 2)
PwoH (n= 2)
HUVEC alone

Figure 6

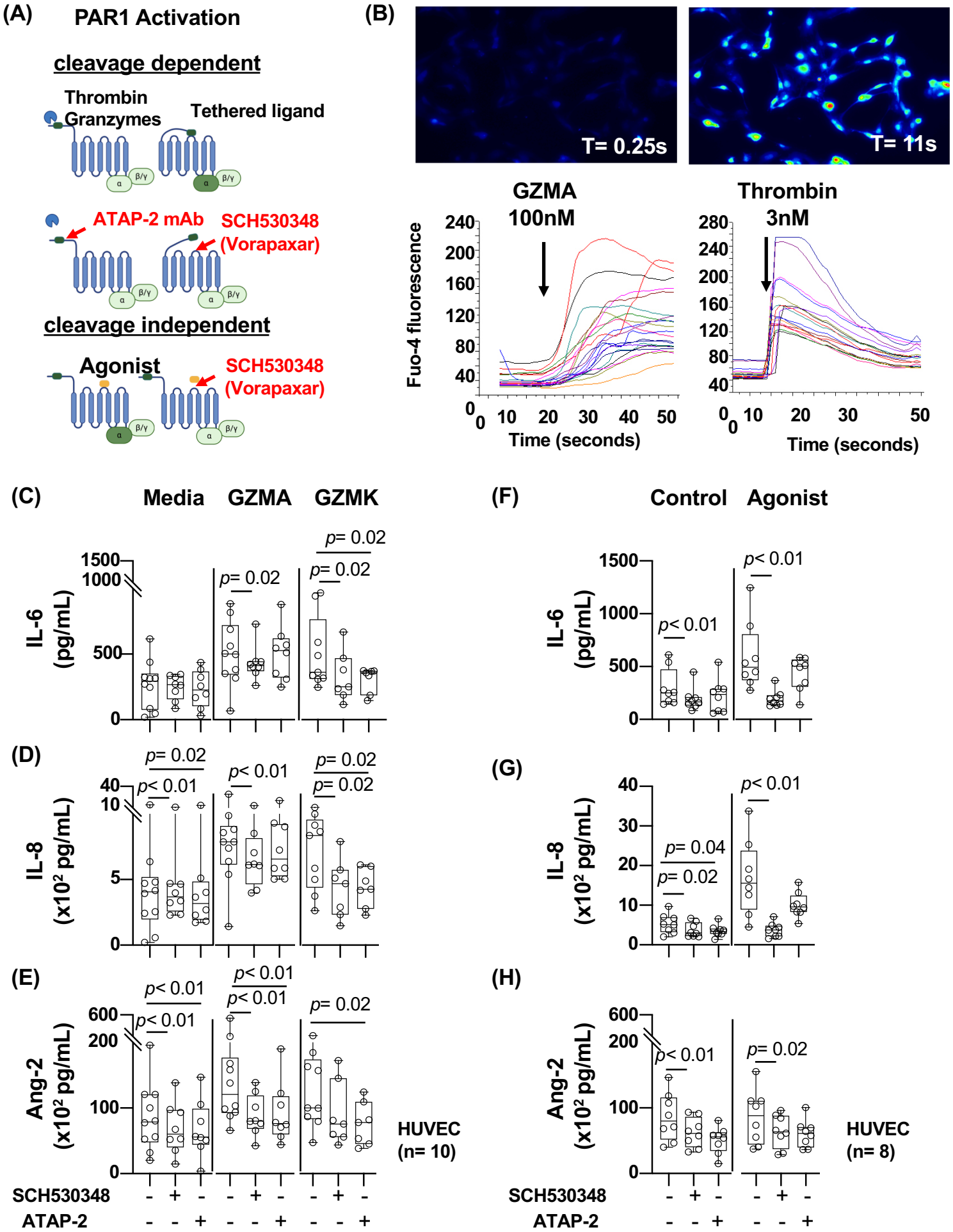
(A)
PAR1 Activation
cleavage dependent
Thrombin
Granzymes
Tethered ligand
ATAP-2 mAb
SCH530348
(Vorapaxar)
cleavage independent
Agonist
SCH530348
(Vorapaxar)
(B)
T= 0.25s
T= 11s
GZMA
100nM
Thrombin
3nM
Fuo-4 fluorescence
Time (seconds)
(C)
Media
GZMA
GZMK
IL-6
(pg/mL)
(D)
IL-8
(x10² pg/mL)
(E)
Ang-2
(x10² pg/mL)
HUVEC
(n= 10)
SCH530348
ATAP-2
(F)
Control
Agonist
(G)
(H)
HUVEC
(n= 8)